UNIVERSITÀ DI PARMA

UNIVERSITA' DEGLI STUDI DI PARMA

Ph.D. in Biotechnology and Life Science

XXXII cycle

Cellular and molecular approaches to the study of Erdheim-Chester Disease and Chronic Periaortitis

Coordinator:
Prof. Simone Ottonello

Tutor:
Prof. Gabriella Moroni

Ph.D. student: Maria Nicastro

2016/2019

To my family

to my beloved Domenico and Diletta

"may knowledge set you free to choose what you believe in"

Contents

Cellular and molecular approaches to the study of Erdheim-Chester Disease and Chronic Periaortitis

Overview of Fibroinflammatory Disorders

Fibroinflammatory disorders are heterogeneous conditions characterized by the deposition of varying amounts of fibrous tissue along with a chronic inflammatory infiltrate. Hence, the normal morpho-functional architecture of a given parenchyma is partially or totally replaced by these fibrosing masses, which are capable of interfering with normal organ function and causing important complications. In addition, the sclerotic masses may sometimes infiltrate structures adjacent to the target organs. This is especially critical in multifocal systemic disorders and especially in cases characterized by particular aggressiveness, such as neoplastic fibro-inflammatory diseases. A further point to be highlighted is the relatively slow turnover of the above-mentioned newly formed tissue, first and foremost fibrosis. This fact makes most clinical treatments scarcely effective in helping to induce *restitutio ad integrum* of the affected anatomical locations.

The nature of these disorders is different and includes idiopathic forms, neoplastic lesions, and reactive processes. Of note, some of these disorders can also be associated with autoimmune diseases. The most frequent fibroinflammatory diseases are sclerosing cholangitis, Riedel's thyroiditis, orbital pseudotumor, sclerosing mesenteritis, and retroperitoneal fibrosis.[1]

The Nephrology Unity at Parma University Hospital is a reference centre for a number of rare diseases including fibroinflammatory disorders such as idiopathic retroperitoneal fibrosis – a condition within the spectrum of chronic periaortitis – and Erdheim-Chester disease.

Erdheim-Chester disease is a disorder included in the clinico-radiological differential diagnosis of chronic periaortitis, because of similar signs/symptoms and computed tomography/magnetic resonance imaging findings (**figure 1**). In fact, both of these diseases are capable of depositing fibrous tissue in the periaortic and perirenal spaces with frequent ureter

entrapment and consequent obstructive uropathy and renal damage. [2, 3]

This PhD thesis comprises two studies on the pathogenesis of Erdheim-Chester disease and chronic periaortitis, respectively. Their aims were to provide new insights into the mechanisms at the basis of abundant fibrous tissue deposition and inflammatory infiltrate organization. Both of these investigations were performed at the Nephrology Unity research laboratory.

REFERENCES

1. Vaglio A and Manenti L. Introduction of fibroinflammatory Disease. In: A. Vaglio, ed. *Sistemic Fibroinflammatory Disorders*. 1st ed. Cham, Switzerland; Springer 2017 ix-xi.
2. Urban ML, Palmisano A, Nicastro M, Corradi D, Buzio C and Vaglio A. Idiopathic and secondary forms of retroperitoneal fibrosis: a diagnostic approach. Rev Med Interne. 2015;36:15-21.
3. Diamond EL, Dagna L, Hyman DM, Cavalli G, Janku F, Estrada-Veras J, Ferrarini M, Abdel-Wahab O, Heaney ML, Scheel PJ, Feeley NK, Ferrero E, McClain KL, Vaglio A, Colby T, Arnaud L and Haroche J. Consensus guidelines for the diagnosis and clinical management of Erdheim-Chester disease. Blood. 2014;124:483-92.

Project 1 – Pro-collagen type I expression in foamy histiocytes in Erdheim-Chester Disease

ABSTRACT

Background. Erdheim-Chester disease (ECD) is a rare systemic disorder characterized by skeletal and extra-skeletal areas where the normal local tissue architecture is replaced by foci of $CD68^{+}/CD1a^{-}$ foamy histiocytes located in a fibrous extracellular matrix. In these foci, the fibroblastic component is often quantitatively minor, notwithstanding the large amounts of fibrous tissue. The aim of this study was to explore whether ECD histiocytes can synthesize collagen type I (Col I) mRNA and subsequently produce this protein.

Methods. In this study we clinico-pathologically investigated 10 ECD biopsies and 10 non-ECD xanthomas biopsies (as non-ECD foamy histiocyte lesions). An ultrastructural examination of the ECD biopsies was performed at the time of the original diagnosis. Two anti-pro-collagen I (pro-col I) and anti-PPAR-γ antibodies were immunohistochemically tested in all of the biopsies and in the ECD samples, respectively. Confocal microscopy was performed to evaluate whether ECD histiocytes co-expressed pro-col I and the histiocytic marker CD68-KP1. Two ECD cases and 6 non-ECD xanthomas underwent real time-polymerase chain reaction (RT-PCR) performed after microdissecting histiocytic tissue areas, to explore the ability of these cells to express the collagen genes *COL1A1* and *COL1A2*. Lastly, RNA In Situ Hybridization (RNA-ISH) was carried out in the 10 ECD cases to morphologically detect the expression of *COL1A1* and *COL1A2* genes.

Results. On electron microscopy, sparse thread-like fibrils in keeping with Col I were found in the cytoplasm of the ECD histiocytes. Immunohistochemical analysis showed a strong expression of pro-col I in ECD histiocytes but a negative signal in foamy histiocytes of non-ECD xanthomas. The PPAR-γ antibody was positive in the nucleus of ECD histiocytes. On confocal microscopy, pro-col I and CD68-KP1 co-expressed in the ECD histiocytes. The RT-

PCR analysis showed that the *COL1A1* and *COL1A2* transcripts were present in the ECD histiocytes, while they were undetectable in the histiocytes of the non-ECD xanthomas. In all ECD cases, the RNA-ISH analysis displayed a very high signal for *COL1A1* and *COL1A2* genes.

Conclusions. In this study we demonstrate that the ECD foamy cell, while retaining a histiocytic phenotype, is capable of expressing Col I genes and synthetizing the relative proteins, thereby mimicking a functionally histiocyte/fibroblast hybrid cell. Future developments of this investigation will aim at investigating the pathogenetic mechanisms of foamy phenotype development, Col I synthesis, and Col I gene mRNA post-transcriptional regulation.

INTRODUCTION

Erdheim-Chester disease (ECD) is an exceedingly rare systemic disorder with approximately 750 reported cases in the literature.[4] The majority of these patients were between 40 and 70 years of age, and were predominantly male (73%); however, some paediatric cases have also been described.[5] ECD occurs clinically with a broad spectrum of manifestations, ranging from a focal isolated to a diffuse infiltrative disease, which often affects multiple organ systems and has a high mortality rate. Extremely frequent possible ECD manifestations include skeletal involvement, diabetes insipidus, exophthalmos, xanthelasmas, retroperitoneal fibrosis with perirenal and/or ureteral involvement, interstitial lung disease, bilateral adrenal enlargement, renal function impairment, testis infiltration, central nervous system and/or cardiovascular involvement. The latter two represent major prognostic factors, as well as independent predictors of death.[6, 7] From an histopathological standpoint, ECD is characterized by skeletal and extraskeletal areas where the normal local tissue architecture has been replaced by foci of $CD68^{+}$ /$CD1a^{-}$ foamy histiocytes.

ECD diagnosis is based on radiological evidence of a symmetrical bilateral skeletal involvement of the long bones plus evidence of the histiocytic infiltrate described above. [8]

The pathogenesis of ECD is still unclear. In 1930, Jakob Erdheim and William Chester first described ECD as a "lipoid granulomatosis".[9] In 1987, the Working Group of the Histiocyte Society (HS), classified histiocytosis in three main categories: Langerhans cell (LC) or non-LC-related (non-LC), and malignant histiocytosis (MH). At that time, ECD was included in non-LC on the basis of histological and immunophenotypical features of the histiocytes.[10]

Over the past few years, many studies have investigated the clonal nature of infiltrating

histiocytes and current observations have demonstrated that 50% of ECD cases harbour the V600E mutation of the *BRAF* proto-oncogene.[11] Other reports have shown *MAP2K1*, *NRAS*, *KRAS* or *PIK3CA* mutations being involved in this disorder thereby indicating that ECD may be clonally driven.[9, 12-14] Furthermore, it has been found that 20% of ECD patients display concomitant Langerhans cell histiocytosis (LCH) lesions. For these reasons, in 2016 the Histiocyte Society reviewed the classification of histiocytosis and suggested including ECD in a broader Langerhans cell group.[5] Immune-mediated mechanisms are also of pathogenetic importance.[15] It has been demonstrated that $CD68^+$ histiocytes express a phosphorylated form of mTOR and p70S6K. [16]

Various therapeutic approaches have been employed for ECD. Interferon-α is considered a first-line therapy, but is often ineffective and poorly tolerated. In addition, the recent acknowledgment of the mutations of certain genes has encouraged the use of specific inhibitor drugs. [17]

The great majority of our ECD patients typically show dyslipidemic features in terms of higher levels of cholesterol and/or triglycerides. Data in the literature have demonstrated that, in *vitro*, $CD14^{high}$ monocytes differentiate into $CD14^{low}$ $CD1a^-$ in the presence of serum lipoproteins. On the contrary, removal of lipoproteins skews their differentiation into $CD1a^+$ cells. Notable, development of $CD1a^-$ monocyte cell is associated with the expression of peroxisome proliferator-activated receptor-gamma (*PPAR-γ*) gene. These results suggest a link between lipoprotein-mediated modulation of monocyte subtype differentiation, PPAR-γ activation, and the functioning of $CD1a^-$ and $CD1a^+$ cells.[18] Interestingly, it has been demonstrated that PPAR-γ has a favourable influence on cholesterol accumulation and accelerates foam-cell formation.[19]

Based on our everyday pathology experience, the fibroblastic component in the ECD foci is frequently minor, even in cases with extensive collagen fibre matrix formation. All these data suggest that in ECD lesions, other cell types contribute to fibrosis in addition to fibroblasts.

Collagen chains are synthesized as a longer precursor, named pro-collagen. The growing peptide chains are co-translationally transported into the lumen of the rough endoplasmic reticulum where the pro-collagen chain undergoes a series of processing reactions. After pro-collagen type I (pro-col I) has been processed and assembled, it is secreted into the extracellular space where extracellular enzymes (so-called "pro-collagen peptidases") remove the N-terminal and C-terminal propeptides. The resulting protein – often called tropocollagen (or simply collagen) – is now able to polymerize into normal fibrils in the extracellular space. [20-22] The aim of this study was to detect pro-col I protein and verify pro-collagen gene expression (*COL1A1* and *COL1A2*). This is an obligatory step to identify the presence of cells other than fibroblasts capable of producing collagen type I (Col I).

METHODS

Patients and controls

We enrolled in this study 10 ECD patients aged between 20 and 75 years, recently diagnosed, and referred to the Nephrology Unity of Parma University Hospital between December 2016 and December 2018. The ECD diagnoses were based on Veyssier-Belot criteria[23]. The exclusion criteria include neoplasms, other histiocytosis forms and infections.

We evaluated 10 diagnostic ECD biopsies, 10 non-ECD xanthomas (benign soft tissue tumours composed of non-ECD foamy histiocytes) as non-ECD foamy histiocyte lesions and as positive controls 2 reparative fibroses consisting of a large number of fibroblasts. All the above-mentioned lesions were paraffin-embedded biopsies obtained from the Unit of Pathology. For each ECD patient, we collected data regarding gender, age, treatment, ECD anatomical sites and possible gene mutations. The study was performed in accordance with the Declaration of Helsinki and was approved by the Ethical Committee.

Ultrastructural examination

Ten small fragments from ECD patients were cut from the samples before morphological analysis to perform an ultrastructural examination. These fragments were fixed in a 4% paraformaldehyde and 5% glutaraldehyde in 0.1 M phosphate buffer (pH 7.3) for 3 hours at room temperature, then in 1% osmium tetroxide. After this, the specimens were dehydrated and embedded in araldite. Sections were cut at 1mm and stained with methylene blue and safranin. After selecting appropriate fields, the sections were collected and laid on a 300-mesh copper grid, then stained with uranyl acetate and lead citrate. Finally, the slides were examined by a transmission electron microscope (Philips, EM 208S, Eindhoven, NL).

Biopsy evaluation and analysis of pro-collagen I and PPAR-γ

All of the ECD and non-ECD biopsies were reviewed on haematoxylin-eosin stained slides and with immunohistochemical analysis for an anti-CD68-KP1 primary antibody in order to confirm the original diagnosis and describe the specific general pathological picture. Subsequently, to evaluate whether pro-col I and PPAR-γ were expressed in ECD histiocytes, we performed immunohistochemical analysis. Ten ECD and 10 non-ECD xanthoma formalin-fixed, paraffin-embedded (FFPE) biopsy specimens were sectioned at 5μm and tested by immunohistochemistry with a pro-col I antibody (code MAB1912, monoclonal, dilution 1:50; Millipore, Darmstadt, DE). Ten ECD biopsies were analysed by testing an antibody against PPAR-γ (code MAB2435, polyclonal, 1:200; Cell Signaling, Leiden, WZ). In the ECD sections, for the PPAR-γ antibody we used the nucleus of the infiltrated adipose cells as a positive control.

Briefly, to remove the paraffin, the slides were immersed in xylene, rehydrated in a decreasing scale of alcohols, and, then put into distilled water. To quench endogenous peroxidase the specimens were treated with a 3% H_2O_2 water solution and then incubated with a protein block (Ready to Use, Dako Biotin Blocking System, Glostrup, DK). The slides were subsequently incubated with the primary antibody for 30 minutes at room temperature and, in sequence, with anti-rat HRP (Polyclonal anti-rat Immunoglobulins/HRP, P0450, Dako) for pro-col I antibody and biotinylated link antibody, and streptavidin-HRP (LSAB2 System, K0675, Dako) for PPAR-γ antibody. Between the above reactions we washed with distilled water. All of these reactions were revealed using 3.3’ diaminobenzidine (DAB) and then counterstained with Harris haematoxylin. The samples were examined with a bright light microscope (Nikon Eclipse 80i, Tokyo, JPN).

Confocal microscopy

Confocal microscopy was performed to evaluate whether ECD histiocytes co-expressed pro-col I and CD68-KP1 (histiocyte marker). Ten ECD tissue sections were deparaffinised as described for the immunohistochemical technique and incubated with a protein block. Then the slides were incubated overnight at 4°C with a CD68-KP1 primary antibody (code ab955, monoclonal, dilution 1:50; Abcam, Cambridge, UK) and its expression the day after was revealed by a fluorescent probe (fluorescein isothiocyanate-conjugated goat anti-mouse IgG, code AP124F, dilution 1:70; Millipore, Massachusetts, USA). After this, we re-incubated the sections with pro-col I primary antibody (MAB1912, monoclonal, dilution 1:10; Millipore) overnight at 4°C. The reactions were determined using a tetramethylrhodamine probe (rhodamine-conjugated goat anti-rat IgG, code AP136R, dilution 1:70; Millipore). Both fluorescent probes were incubated for 1 hour at room temperature. The final immunofluorescence samples were observed under a confocal system (LSM 510 META scan head integrated with the Axiovert 200M inverted microscope; Carl Zeiss) with an x63 oil objective. The images were acquired in multitrack mode, using consecutive and independent optical pathways.

Laser capture microdissection

Only those cases that presented histiocytes or fibroblasts organised into homogeneous groups were considered suitable for laser capture microdissection (LCM). On this basis, only 2 ECD cases, 6 non-ECD xanthomas, and 2 reparative fibroses were used to perform LCM analysis. FFPE sections for each sample were cut at 5μm and placed on metal frame slides with thermoplastic membrane (Molecular Machines & Industries AG; Glattburg, Zurich, Switzerland). The slides were dried for 1 hour at 37°C and subsequently for 5 hours at room

temperature. After this, the sections were rehydrated with a decreasing scale of alcohols, washed in RNAse free water and haematoxylin-eosin stained.

The day after preparing the slides, we analysed the sections with a NIKON ECLIPSE-TE 2000 inverted microscope (Nikon-Instruments, Sesto Fiorentino, Italy). NIKON ECLIPSE-TE 2000 consists of a Molecular Machines & Industries Cell cut Laser Capture Microdissection system in which an ultraviolet laser is characterized by high precision cutting that does not damage the tissue. The instruments are linked to a CCD camera, which allowed us to identify and then select the areas of our interest. In each specimen, the areas rich in histiocytes in ECD and non-ECD xanthomas and in fibroblasts in reparative fibrosis biopsies were microdissected. These cells were captured in the adhesive lid of a single isolation cap (Nikon Instruments) (**figure 2**).

RNA extraction

Samples obtained by LCM were extracted with an RNeasy FFPE Kit (code 73504; Qiagen, Hilden, DE) according to the manufacturer's instructions (see the RNeasy® FFPE Handbook, Qiagen, page 17).

The RNeasy FFPE Kit was recommended for RNA extraction from FFPE tissue and in particular for microdissected samples. The Kit provides a DNase digestion step that is indispensable to remove DNA contamination.

Briefly, the first step concerned the elimination of paraffin from specimens using a Deparaffinization Solution at 56°C for 5 minutes. The samples were incubated in PKD buffer and proteinase K at 56°C for 15 minutes, then at 80°C for 15 minutes. The incubation with proteinase K at a higher temperature is necessary to break cross-links formed between formalin and active groups of proteins and released RNA. The second important step consisted of the

elimination of all genomic DNA added a DNase treatment at room temperature for 15 minutes. Then, buffer RBC and ethanol were added to the lysate to improve the binding conditions of DNase. The eluate was transferred to an RNeasy MinElute spin column, where total RNA binds to the membrane. All of the contaminants were eliminated by carrying out various washes. The RNA was then eluted in a 30µl of RNase-free water.

After extraction, the RNA was placed in a new tube and checked for integrity and purity by Nanodrop spectrophotometer (Thermo Scientific, Massachusetts, USA), and immediately frozen at -80 °C.

Real time-polymerase chain reaction

A cDNA synthesis was performed using a commercial kit, which includes inverse transcriptase (Life Technologies, California, USA). For each sample, 2µl of 2xRT Buffer Mix, 1µl of RT Enzyme Mix and 100ng of RNA were combined to reach a final volume of 20µl. Then the samples were incubated at 37°C for 60 minutes and at 95°C for 5 minutes. At the end of the reaction, the samples of cDNA were diluted 1:2 in H_2O RNase free (Ambion). The cDNA was amplified by real time-polymerase chain reaction (RT-PCR) on an iCycler iQ Multicolor RT-PCR Detection System (Bio-Rad, Hercules, CA, USA) using specific primers including exon-exon junctions and probe FAM-labelling specifically designed for *Collagen type I alpha chain* (*COL1A1*, cod. 04688678001, Roche Life Science, Penzberg, DE) and *Collagen type I alpha 2 chain* (*COL1A2,* cod. 0489020001, Roche Life Science). The reaction mix consisted of 2µl of previously diluted cDNA, 400nM of forward primers and reverses specific to each gene, 0.1µM of probes, TaqMan 2x Universal PCR Master Mix (Life Technologies) and H_2O for a final volume of 25µl. Duplicate assays were run for each sample and each plate included a negative control. After normalization with phosphoglycerate kinase 1 (PGK1, cod.

04688686001, Roche Life Science) housekeeping gene, the expression of the transcripts was calculated by $2^{-\Delta Ct}$. RT-PCR was performed on all microdissected cases.

RNA In Situ Hybridization

RNA In Situ Hybridization (RNA-ISH) was carried out using an RNAscope® 2.5 Assay in 10 ECD FFPE cases (8 unsuitable and 2 suitable for LCM) (**figure 3**). In these 2 suitable samples, RNA-ISH also served to confirm the results obtained by RT-PCR. In addition, we detected histiocytic expression of *COL1A1* and *COL1A2* genes on a morphological basis. For this method the protocol provided by the company was carefully followed [see RNAscope® 2.5 Assay Detection Kit (Red), Quick Guide for FFPE Tissues-Advanced Cell Diagnostics (ACD), Newark, CA]. The RNAscope® 2.5 Assay is a new method used to identify a single RNA molecule also in specimens from FFPE tissues. This technology uses specific probes that hybridize with high specificity to target RNA. Briefly, the FFPE of 10 ECD samples were cut at 5μm thickness and placed on superfrost plus slides. The specimens were air-dried overnight at room temperature and then placed at 60°C for 1 hour. Subsequently, the sections were deparaffinised using xylene and ethanol and air-dried overnight at room temperature. This procedure includes the use of pre-treatment reagents to make target RNA accessible. As a first pre-treatment we applied hydrogen peroxide for 10 minutes at room temperature to block endogenous peroxidase activity. Then we added to the slides a target retrieval for 15 minutes at 99°C and finally protease plus reagents for 30 minutes at 40°C. These passages are necessary to break any cross-links that occur after tissue fixation. Between the pre-treatment passages slides were washed with distilled water.

For each case a specific probe [HsCOL1A1 (ref. 401891; lot. 18207A), HsCOL1A2 (ref. 432721; lot. 8081A)] was used to identify collagen genes, and also a PPIB (peptidylprolyl

isomerase B) housekeeping gene positive probe and a DapB (bacterial gene) negative control probe. These probes were applied for 2 hours at 40°C in an HybEZ oven. The method included many amplification steps, which are important for genes with low expression and for RNA of old paraffin blocks or degraded samples. In particular, AMP1 for 15 minutes at 40°C, AMP2 for 30 minutes at 40°C, AMP3 for 30 minutes at 40°C, AMP4 for 15 minutes at 40°C, AMP5 for 30 minutes at room temperature, and AMP6 for 15 minutes at room temperature were added; the sections were washed with wash buffer between amplification steps. Subsequently, incubated with Fast Red solution for 10 minutes at room temperature to detect the signal and counterstained with haematoxylin for 2 minutes at room temperature. The slides were washed with 0.02% ammonia water and then in distilled water. It was air-dried for 15 minutes at 60°C and mounted. Finally, the samples were observed with a bright light microscope (Nikon Eclipse 80i, Tokyo, JPN).

RESULTS

Patients

In this study we enrolled 10 patients who had undergone a biopsy to confirm the clinico-radiological diagnosis of ECD. All patients were untreated at the time of biopsy. In these patients we evaluated which organs were involved by the pathology and we investigated the presence of some mutations. We found retroperitoneal involvement in seven patients with fibrous masses that surrounded the aorta, kidney, and ureter. Cardiac and lung involvement was observed in 4 cases, while CNS involvement was found in 2. Endocrine abnormalities were detected in 5 patients. Symmetrical bilateral skeletal involvement of the long bones was found in 9 cases. Other less frequent lesions, such as skin and testis infiltration, exophthalmos, bilateral adrenal enlargement, were also seen.

In these patients, we analysed the principal mutations described in literature such as *BRAF*^{V600E}, and others involving *NRAS*, *KRAS* or *PIK3CA*. We found that 6 of the ECD patients were positive for the *BRAF*^{V600E} mutation, 2 did not have any mutation while in 2 cases we were unable to obtain these data. These findings are summarized in **table 1**.

Ultrastructural examination

We examined 10 ECD cases with additional samples taken for electron microscopy analysis. At a lower power view, we found regular foamy histiocytes located in collagen-rich extracellular matrix. Interestingly, at higher magnification we detected in the cytoplasm of the same foamy histiocytes sparse thread-like fibrils with light and dark cross-striations which were highly in keeping with Col I (**figure 4**).

Tissue expression of pro-collagen I and PPAR-γ

The re-evaluation of all biopsies confirmed the original diagnosis (**figure 5**). Histiocytes were a major infiltrate in fibrous tissue of ECD foci. To better understand whether histiocytes were positive for pro-col I and PPAR-γ we applied immunohistochemical analysis. We detected a strong expression of pro-col I in ECD histiocytes but a negative signal in foamy histiocytes of non-ECD xanthomas (**figure 6**). Subsequently, we found that the PPAR-γ antibody was positive in the nucleus of ECD histiocytes which had infiltrated the tissues, and in the nucleus of the adipose cells. We used the latter as an internal positive control (**figure 7**). After, we evaluated by confocal microscopy the co-expression of pro-col I and CD68-KP1 (histiocyte marker) in 10 ECD biopsies. This analysis showed that the ECD histiocytes co-localized for the above-mentioned proteins (**figure 8**).

***COL1A1* and *COL1A2* gene expression**

The expression of collagen genes (*COL1A1* and *COL1A2*) was analysed by RT-PCR in the histiocytes of 2 ECD cases, in 6 non-ECD xanthomas, and in fibroblasts (used as positive controls) of 2 reparative fibroses. All of these samples were obtained from FFPE diagnostic biopsies, as described above. The *COL1A1* and *COL1A2* transcript levels were noticeably higher in the ECD histiocytes and control fibroblasts, while the histiocytes of the non-ECD xanthomas were negative (**figure 9**).

Overexpression of *COL1A1* and *COL1A2* gene by RNA In Situ Hybridization

In all ECD cases, using RNA-ISH the histiocytes showed a very high signal related to *COL1A1* and *COL1A2* genes. The presence of reddish clusters in the ECD cases – compared to the small dots in the positive controls – was indicative of significant gene expression. The

tissues and cells surrounding the histiocytes were negative for pro-col I genes. In all the ECD cases, we also tested the PPIB probe, as a housekeeping gene, and a DapB, as a negative control probe provided by an RNA-ISH kit. In the ECD cases, the PPIB housekeeping gene displayed positivity in terms of small dots while the DapB probe gene was always negative (**figure 10**). These results demonstrated that the expression of all the genes was target-specific and in keeping with the principle of this method according to which a double Z probe (RNAscope® Manual Reagents, Gene Expression Analysis by RNA In Situ Hybridization, ACD, pp. 4,5) is designed for each precise target.

DISCUSSION

ECD is a rare – though still pathogenetically indefinite in its details – systemic disorder characterized by foci of foamy histiocytes located in varying amounts of Col I-rich fibrous tissue. Depending on both the extent of the ECD lesions and the anatomical location involved, the above-mentioned disease foci often greatly interfere with organ function and, at the same time, may represent the basis for major complications.[6]

Based on routine experience gained over the past few years at our centre, the fibroblastic component in the ECD foci is frequently minor, even in cases with extensive collagen fibre matrix formation. This is why, in our study we investigated whether foamy histiocytes – which represent a prominent cellular component in the ECD foci – are able to synthetize and produce Col I. To this end, we first analysed ECD cases that had provided an additional sample for electron microscopy analysis. Interestingly, at higher magnification, we were able to ultrastructurally detect in the cytoplasm of foamy histiocytes sparse thread-like fibrils that were strongly in keeping with Col I. These intracellular fibrils seemed to be truly new-formed Col I protein complexes and not a mere result of a phagocytosis process. Hence, a fundamental question is whether, in particular conditions, monocyte-derived cells and macrophages act as functionally hybrid elements with capacities typical of both macrophages and fibroblasts but a histiocytic phenotype.

Data from the scientific literature have frequently shown that monocytes and macrophages possess a functional/molecular plasticity and, in addition, are able to express many types of collagen.[24] [25] In fact, the existence of cells with coexisting features (both morphological and functional) of fibroblasts and macrophages has been described for many years.[26-29] Inter-conversion of fibroblasts into macrophage/monocytes and vice versa has long

been demonstrated in the cornea and skin, and blood monocytes have been proven to be capable of switching into fibroblasts, *in vitro*.[28, 30, 31] More recently, it has been seen that in chronic kidney disease, macrophages could be involved in macrophage-to-mesenchymal transition phenomena and, as a consequence, in collagen formation. In particular, these cells were found to have co-expressed the macrophage marker CD68 and the myofibroblastic marker α-SMA.[24, 32, 33] A further similar observation was made on tumour-associated macrophages, which have been shown to greatly contribute to local collagen deposition.[34, 35]

Based on our ultrastructural findings and the above-described scientific evidence, the aim of this study was to explore whether ECD histiocytes are capable of synthesizing Col I mRNA and, as a consequence, of producing this protein. We demonstrated both by RT-PCR and RNA-ISH that ECD histiocytes express the *COL1A1* and *COL1A2* genes. Subsequently, in ECD biopsies we found that these cells showed a strong immunohistochemical positivity for pro-col I protein. Our data seem to prove that ECD histiocytes are not the result of a transdifferentiative process; in fact, they retain the phenotypical characteristics of foamy histiocytes, and, at the same time, acquire the typical capacity of fibroblasts to product Col I. This latter evidence has been supported by the co-expression in these ECD cells of CD68 and pro-col I using confocal microscopy. On the contrary, non-ECD histiocytes in xanthomas did not express collagen protein with immunohistochemistry nor did the Col I chains with RT-PCR.

Having established that ECD foamy histiocytes are capable of synthesising Col I, a further step was to identify the specific mechanisms leading to the accumulation of these cells in the disease foci and, successively, those that make these cells capable of secreting collagen.

Curiously, we noticed that our ECD patients displayed dyslipidemic features. In the scientific literature, a few case report studies – and with contrasting observations - dealt with lipid metabolism in ECD patients.[36-38] Only a recent investigation, performed in a large

monocentric cohort of ECD patients, analysed the plasma lipid levels in 60 males and 18 females and found that hypoalphalipoproteinemia in male *BRAF*^{V600E}-mutated ECD patients would favour the development of foamy histiocytes.[39]

We also found that ECD histiocytes were immunohistochemically positive for PPAR-γ, a major regulator of adipogenesis as well as a potent modulator of systemic lipid metabolism and insulin sensitivity.[40] Furthermore, it has been described that monocytes can acquire a specific immunophenotype- CD14^{low}/CD1a^{-} -in the presence of serum lipoproteins and also express the *PPAR-γ* gene that seems to promote cholesterol accumulation and formation of cells with foamy morphology.[18, 19] It would be relevant to extend our patient population in order to investigate the lipid metabolism in patients carrying any type of mutation and in cases without gene alterations and to understand if the presence of cholesterol/triglycerides in the serum of ECD patients could truly increase the formation of foamy histiocytes.

Additionally, it is well known that macrophages express arginase. Arginase is involved in the conversion of L-arginine into urea and L-ornithine, and the latter, in turn, is converted into polyamines and L-proline, which is an essential amino acid for collagen formation.[41] It has already been shown that many diseases characterised by collagen deposition have an increased activity of arginase. [42, 43] In accordance with these observations, some studies have concluded that arginase expression would be favoured by the presence of serum lipoproteins and PPAR-γ activation.[44] These data seem to be in line with the findings of our study.

In order to clarify this hypothesis, a further step of our study could be culturing monocytes using the patients' sera to explore whether they are able to develop a foamy-cell phenotype and express the *PPAR-γ* gene. Moreover, it would also be intriguing to compare the expression of arginase and L-ornithine in ECD foamy histiocytes vs. non-ECD histiocytes to identify whether a different expression exists; in fact, greater arginase expression could increase

the bioavailability of polyamines and proline which, as already noted, is essential for collagen synthesis.[45]

With regard to the specific cellular regulations involved in the exuberant Col I production by foamy histiocytes, since no Col I gene alterations have been described in ECD, another study stemming from this investigation would be to explore the exact functional location where the Col I synthesis is altered in terms of increased protein production at its transcriptional and/or post-transcriptional level.

The collagen percentage synthesis per hour (so-called "constitutive fractional synthesis rate") is slower than that of most proteins in our body [46, 47] However, this rate considerably increases (greater than 300-fold) in case of acute protein requests (*e.g.* in reparative fibrosis) or reactive fibrotic processes (*e.g.* pathological scarring processes of specific organs in fibroinflammatory disorders).[48] Early studies aimed at exploring the dramatic increase in Col I synthesis based exclusively on the transcriptional regulation showed that it is not possible to reproduce quantitative and tissue specific aspects of Col I expression by utilizing only the transcription controlling elements.[49-51] In addition, *in vitro* studies on activated hepatic stellate cells (HSC; with 50-100-fold increase in collagen synthesis) demonstrated that the rate of transcription of the *COL1A1* gene was increased only 3-fold.[52] The above-mentioned scientific evidence suggested that, most likely, the collagen expression is primarily regulated at a post-transcriptional level, including regulation of half-life and translation of collagen mRNAs.[53] In this context, the La ribonucleoprotein domain family, member 6 (LARP6), an RNA binding protein belonging to the LARP protein superfamily, has come to prominence as one of the most promising regulators of Col I synthesis. In fact, this protein is capable of binding the conserved structural element in the 5′ UTR of *COL1A1* and *COL1A2* mRNAs (5′ stem-loop) (5′ SL), a 48 nucleotide-long stem-loop structure. In cytoplasm, LARP6 associates collagen mRNA with

vimentin filaments (leading to collagen mRNA stabilization) or with non-muscle myosin filaments (supporting collagen mRNA translation). In addition, LARP6 tethers stimulatory factors, such as RNA helicase (RHA), serine/threonine kinase receptor associated protein (STRAP) or FK506 binding protein (FKBP3) to collagen mRNAs to increase their translational competitiveness. No further RNA, other than collagen type III, has been identified to which LARP6 can bind with high affinity, classifying LARP6 as a specific RNA binding protein of collagen mRNAs.[54] Intriguingly, it has recently been shown that mTORC1 is able to phosphorylate LARP6 on S348 and S409 and that the S348A/S409A mutant of LARP6 acts as a dominant negative protein in collagen biosynthesis, which retards secretion of Col I, thereby causing excessive post-translational modifications.[53] Of note, in biopsies from our own ECD patients, we found that the histiocytes expressed a phosphorylated form of mTOR and the downstream kinase p70S6K.[16] The above-discussed evidence that binding of LARP6 to the 5′SL sequence of Col I mRNAs is a key factor for fibrosis development opened the possibility that profibrotic production of Col I can be specifically targeted. Very recently, an elegant *in vitro* and *ex vivo* investigation by Stefanovic et al. found that the "screen yielded one compound" (also known as C9) was able to dissociate LARP6 from 5′ SL RNA probably by inducing a conformational modification in this protein. In prophylactic and therapeutic animal models of hepatic fibrosis, C9 compound prevented development of fibrosis or impeded the progression of ongoing fibrosis.[55]

Conclusions and future developments

In this study, we demonstrated that the ECD foamy cell, while retaining a complete histiocytic phenotype, is capable of expressing Col I genes and synthetizing the relative proteins, thereby featuring the characteristics of a functionally histiocyte/fibroblast hybrid cell.

Future developments of this study aimed at investigating the pathogenetic mechanisms of this collagen production might include: a) the role of PPAR-γ in the potential induction of a foamy-cell phenotype in culturing monocytes from ECD patients, b) exploring in ECD foamy histiocytes the arginase and L-ornithine expression and their possible role in increasing the bioavailability of proline, and c) the potential role of LARP6 in the post-transcriptional regulation of *COL1A1* and *COL1A2* mRNAs.

REFERENCES

4. Stempel JM, Bustamante Alvarez JG, Carpio AM, Mittal V and Dourado C. Erdheim-Chester disease, moving away from the orphan diseases: A case report. Respir Med Case Rep. 2017;20:55-58.
5. Emile JF, Abla O, Fraitag S, Horne A, Haroche J, Donadieu J, Requena-Caballero L, Jordan MB, Abdel-Wahab O, Allen CE, Charlotte F, Diamond EL, Egeler RM, Fischer A, Herrera JG, Henter JI, Janku F, Merad M, Picarsic J, Rodriguez-Galindo C, Rollins BJ, Tazi A, Vassallo R, Weiss LM and Histiocyte S. Revised classification of histiocytoses and neoplasms of the macrophage-dendritic cell lineages. Blood. 2016;127:2672-81.
6. Haroche J, Arnaud L and Amoura Z. Erdheim-Chester disease. Curr Opin Rheumatol. 2012;24:53-9.
7. Goyal G, Young JR, Koster MJ, Tobin WO, Vassallo R, Ryu JH, Davidge-Pitts CJ, Hurtado MD, Ravindran A, Sartori Valinotti JC, Bennani NN, Shah MV, Rech KL, Go RS and Mayo Clinic Histiocytosis Working G. The Mayo Clinic Histiocytosis Working Group Consensus Statement for the Diagnosis and Evaluation of Adult Patients With Histiocytic Neoplasms: Erdheim-Chester Disease, Langerhans Cell Histiocytosis, and Rosai-Dorfman Disease. Mayo Clin Proc. 2019;94:2054-2071.
8. Ozkaya N, Rosenblum MK, Durham BH, Pichardo JD, Abdel-Wahab O, Hameed MR, Busam KJ, Travis WD, Diamond EL and Dogan A. The histopathology of Erdheim-Chester disease: a comprehensive review of a molecularly characterized cohort. Mod Pathol. 2018;31:581-597.
9. Durham BH. Molecular characterization of the histiocytoses: Neoplasia of dendritic cells and macrophages. Semin Cell Dev Biol. 2019;86:62-76.
10. Histiocytosis syndromes in children. Writing Group of the Histiocyte Society. Lancet. 1987;1:208-9.
11. Cangi MG, Biavasco R, Cavalli G, Grassini G, Dal-Cin E, Campochiaro C, Guglielmi B, Berti A, Lampasona V, von Deimling A, Sabbadini MG, Ferrarini M, Doglioni C and Dagna L. BRAFV600E-mutation is invariably present and associated to oncogene-induced senescence in Erdheim-Chester disease. Ann Rheum Dis. 2015;74:1596-602.
12. Haroche J, Cohen-Aubart F, Rollins BJ, Donadieu J, Charlotte F, Idbaih A, Vaglio A, Abdel-Wahab O, Emile JF and Amoura Z. Histiocytoses: emerging neoplasia behind inflammation. Lancet Oncol. 2017;18:e113-e125.
13. Ozkaya N, Dogan A and Abdel-Wahab O. Identification and Targeting of Kinase Alterations in Histiocytic Neoplasms. Hematol Oncol Clin North Am. 2017;31:705-719.
14. Papo M, Cohen-Aubart F, Trefond L, Bauvois A, Amoura Z, Emile JF and Haroche J. Systemic Histiocytosis (Langerhans Cell Histiocytosis, Erdheim-Chester Disease, Destombes-Rosai-Dorfman Disease): from Oncogenic Mutations to Inflammatory Disorders. Curr Oncol Rep. 2019;21:62.
15. Arnaud L, Gorochov G, Charlotte F, Lvovschi V, Parizot C, Larsen M, Ghillani-Dalbin P, Hervier B, Kahn JE, Deback C, Musset L, Amoura Z and Haroche J. Systemic perturbation of cytokine and chemokine networks in Erdheim-Chester disease: a single-center series of 37 patients. Blood. 2011;117:2783-90.
16. Gianfreda D, Nicastro M, Galetti M, Alberici F, Corradi D, Becchi G, Baldari G, De Filippo M, Ferretti S, Moroni G, Foti R, Di Gangi M, Jeannin G, Saffroy R, Emile JF, Buzio C and Vaglio A. Sirolimus plus prednisone for Erdheim-Chester disease: an open-label trial. Blood. 2015;126:1163-71.

17. Haroche J, Charlotte F, Arnaud L, von Deimling A, Helias-Rodzewicz Z, Hervier B, Cohen-Aubart F, Launay D, Lesot A, Mokhtari K, Canioni D, Galmiche L, Rose C, Schmalzing M, Croockewit S, Kambouchner M, Copin MC, Fraitag S, Sahm F, Brousse N, Amoura Z, Donadieu J and Emile JF. High prevalence of BRAF V600E mutations in Erdheim-Chester disease but not in other non-Langerhans cell histiocytoses. Blood. 2012;120:2700-3.
18. Gogolak P, Rethi B, Szatmari I, Lanyi A, Dezso B, Nagy L and Rajnavolgyi E. Differentiation of CD1a- and CD1a+ monocyte-derived dendritic cells is biased by lipid environment and PPARgamma. Blood. 2007;109:643-52.
19. Moore KJ, Rosen ED, Fitzgerald ML, Randow F, Andersson LP, Altshuler D, Milstone DS, Mortensen RM, Spiegelman BM and Freeman MW. The role of PPAR-gamma in macrophage differentiation and cholesterol uptake. Nat Med. 2001;7:41-7.
20. Rossert J, Terraz C and Dupont S. Regulation of type I collagen genes expression. Nephrol Dial Transplant. 2000;15 Suppl 6:66-8.
21. Canty EG and Kadler KE. Procollagen trafficking, processing and fibrillogenesis. J Cell Sci. 2005;118:1341-53.
22. Marini JC, Forlino A, Bachinger HP, Bishop NJ, Byers PH, Paepe A, Fassier F, Fratzl-Zelman N, Kozloff KM, Krakow D, Montpetit K and Semler O. Osteogenesis imperfecta. Nat Rev Dis Primers. 2017;3:17052.
23. Veyssier-Belot C, Cacoub P, Caparros-Lefebvre D, Wechsler J, Brun B, Remy M, Wallaert B, Petit H, Grimaldi A, Wechsler B and Godeau P. Erdheim-Chester disease. Clinical and radiologic characteristics of 59 cases. Medicine (Baltimore). 1996;75:157-69.
24. Nikolic-Paterson DJ, Wang S and Lan HY. Macrophages promote renal fibrosis through direct and indirect mechanisms. Kidney Int Suppl (2011). 2014;4:34-38.
25. Poltavets V, Kochetkova M, Pitson SM and Samuel MS. The Role of the Extracellular Matrix and Its Molecular and Cellular Regulators in Cancer Cell Plasticity. Front Oncol. 2018;8:431.
26. Kouri J and Ancheta O. Transformation of macrophages into fibroblasts. Exp Cell Res. 1972;71:168-76.
27. Feigl W, Susani M, Ulrich W, Matejka M, Losert U and Sinzinger H. Organisation of experimental thrombosis by blood cells. Evidence of the transformation of mononuclear cells into myofibroblasts and endothelial cells. Virchows Arch A Pathol Anat Histopathol. 1985;406:133-48.
28. Eyden B. The myofibroblast: a study of normal, reactive and neoplastic tissues, with an emphasis on ultrastructure. J Submicrosc Cytol Pathol. 2007:7-166.
29. Yang J, Lin SC, Chen G, He L, Hu Z, Chan L, Trial J, Entman ML and Wang Y. Adiponectin promotes monocyte-to-fibroblast transition in renal fibrosis. J Am Soc Nephrol. 2013;24:1644-59.
30. Kaye GI and Pappas GD. Studies on the cornea. I. The fine structure of the rabbit cornea and the uptake and transport of colloidal particles by the cornea in vivo. J Cell Biol. 1962;12:457-79.
31. Labat ML, Bringuier AF, Arys-Philippart C, Arys A and Wellens F. Monocytic origin of fibrosis. In vitro transformation of HLA-DR monocytes into neo-fibroblasts: inhibitory effect of all-trans retinoic acid on this process. Biomed Pharmacother. 1994;48:103-11.
32. Srivastava SP, Hedayat FA, Kanasaki K and Goodwin JE. microRNA Crosstalk Influences Epithelial-to-Mesenchymal, Endothelial-to-Mesenchymal, and Macrophage-to-Mesenchymal Transitions in the Kidney. Front Pharmacol. 2019;10:904.

33. Wang S, Meng XM, Ng YY, Ma FY, Zhou S, Zhang Y, Yang C, Huang XR, Xiao J, Wang YY, Ka SM, Tang YJ, Chung AC, To KF, Nikolic-Paterson DJ and Lan HY. TGF-beta/Smad3 signalling regulates the transition of bone marrow-derived macrophages into myofibroblasts during tissue fibrosis. Oncotarget. 2016;7:8809-22.
34. Afik R, Zigmond E, Vugman M, Klepfish M, Shimshoni E, Pasmanik-Chor M, Shenoy A, Bassat E, Halpern Z, Geiger T, Sagi I and Varol C. Tumor macrophages are pivotal constructors of tumor collagenous matrix. J Exp Med. 2016;213:2315-2331.
35. Qiu S, Deng L, Liao X, Nie L, Qi F, Jin K, Tu X, Zheng X, Li J, Liu L, Liu Z, Bao Y, Ai J, Lin T, Yang L and Wei Q. Tumor-associated macrophages promote bladder tumor growth through PI3K/AKT signal induced by collagen. Cancer Sci. 2019;110:2110-2118.
36. Schmidt HH, Gregg RE, Shamburek R, Brewer BH, Jr. and Zech LA. Erdheim-Chester disease: low low-density lipoprotein levels due to rapid catabolism. Metabolism. 1997;46:1215-9.
37. Kujat C, Martin J and Puschel W. [Erdheim-Chester disease]. Radiologe. 1991;31:297-306.
38. Miller RL, Sheeler LR, Bauer TW and Bukowski RM. Erdheim-Chester disease. Case report and review of the literature. Am J Med. 1986;80:1230-6.
39. Cohen-Aubart F, Guerin M, Poupel L, Cluzel P, Saint-Charles F, Charlotte F, Arsafi Y, Emile JF, Frisdal E, Le Goff C, Donadieu J, Amoura Z, Lesnik P, Haroche J and Le Goff W. Hypoalphalipoproteinemia and BRAF(V600E) Mutation Are Major Predictors of Aortic Infiltration in the Erdheim-Chester Disease. Arterioscler Thromb Vasc Biol. 2018;38:1913-1925.
40. Ahmadian M, Suh JM, Hah N, Liddle C, Atkins AR, Downes M and Evans RM. PPARgamma signaling and metabolism: the good, the bad and the future. Nat Med. 2013;19:557-66.
41. Rappu P, Salo AM, Myllyharju J and Heino J. Role of prolyl hydroxylation in the molecular interactions of collagens. Essays Biochem. 2019;63:325-335.
42. Caldwell RB, Toque HA, Narayanan SP and Caldwell RW. Arginase: an old enzyme with new tricks. Trends Pharmacol Sci. 2015;36:395-405.
43. Yang Z and Ming XF. Functions of arginase isoforms in macrophage inflammatory responses: impact on cardiovascular diseases and metabolic disorders. Front Immunol. 2014;5:533.
44. Gallardo-Soler A, Gomez-Nieto C, Campo ML, Marathe C, Tontonoz P, Castrillo A and Corraliza I. Arginase I induction by modified lipoproteins in macrophages: a peroxisome proliferator-activated receptor-gamma/delta-mediated effect that links lipid metabolism and immunity. Mol Endocrinol. 2008;22:1394-402.
45. Kitowska K, Zakrzewicz D, Konigshoff M, Chrobak I, Grimminger F, Seeger W, Bulau P and Eickelberg O. Functional role and species-specific contribution of arginases in pulmonary fibrosis. Am J Physiol Lung Cell Mol Physiol. 2008;294:L34-45.
46. el-Harake WA, Furman MA, Cook B, Nair KS, Kukowski J and Brodsky IG. Measurement of dermal collagen synthesis rate in vivo in humans. Am J Physiol. 1998;274:E586-91.
47. Thalacker-Mercer AE and Campbell WW. Dietary protein intake affects albumin fractional synthesis rate in younger and older adults equally. Nutr Rev. 2008;66:91-5.
48. Stefanovic B. RNA protein interactions governing expression of the most abundant protein in human body, type I collagen. Wiley Interdiscip Rev RNA. 2013;4:535-45.
49. Sokolov BP, Ala-Kokko L, Dhulipala R, Arita M, Khillan JS and Prockop DJ. Tissue-specific expression of the gene for type I procollagen (COL1A1) in transgenic mice. Only

476 base pairs of the promoter are required if collagen genes are used as reporters. J Biol Chem. 1995;270:9622-9.
50. Rossert J, Eberspaecher H and de Crombrugghe B. Separate cis-acting DNA elements of the mouse pro-alpha 1(I) collagen promoter direct expression of reporter genes to different type I collagen-producing cells in transgenic mice. J Cell Biol. 1995;129:1421-32.
51. Slack JL, Liska DJ and Bornstein P. Regulation of expression of the type I collagen genes. Am J Med Genet. 1993;45:140-51.
52. Stefanovic B, Hellerbrand C, Holcik M, Briendl M, Aliebhaber S and Brenner DA. Posttranscriptional regulation of collagen alpha1(I) mRNA in hepatic stellate cells. Mol Cell Biol. 1997;17:5201-9.
53. Zhang Y and Stefanovic B. mTORC1 phosphorylates LARP6 to stimulate type I collagen expression. Sci Rep. 2017;7:41173.
54. Stefanovic L, Longo L, Zhang Y and Stefanovic B. Characterization of binding of LARP6 to the 5' stem-loop of collagen mRNAs: implications for synthesis of type I collagen. RNA Biol. 2014;11:1386-401.
55. Stefanovic B, Manojlovic Z, Vied C, Badger CD and Stefanovic L. Discovery and evaluation of inhibitor of LARP6 as specific antifibrotic compound. Sci Rep. 2019;9:326.

Table

Table 1. Demographic and clinical characteristics of the Erdheim-Chester Disease (ECD) untreated patients included in the study

	ECD patients N=10
Age, years – *median (range)*	44 (26–59)
Male gender, *n (%)*	5 (50)
Clinical manifestations, n (%)	
Retroperitoneal	7 (70)
Cardiac and lung	4 (40)
Central Nervous System	2 (20)
Endocrine abnormalities	5 (50)
Bilateral skeletal involvement of the long bones	9 (90)
Minor involvement*	10 (100)
Mutations, n (%)	
BRAF^{V600E}	6 (60)
NRAS	0
KRAS	0
PIK3CA	0

ECD patients were not undergoing treatment at the time of biopsies

*Minor involvement: skin lesions, testis infiltration, exophthalmos or bilateral adrenal enlargement.

Figures

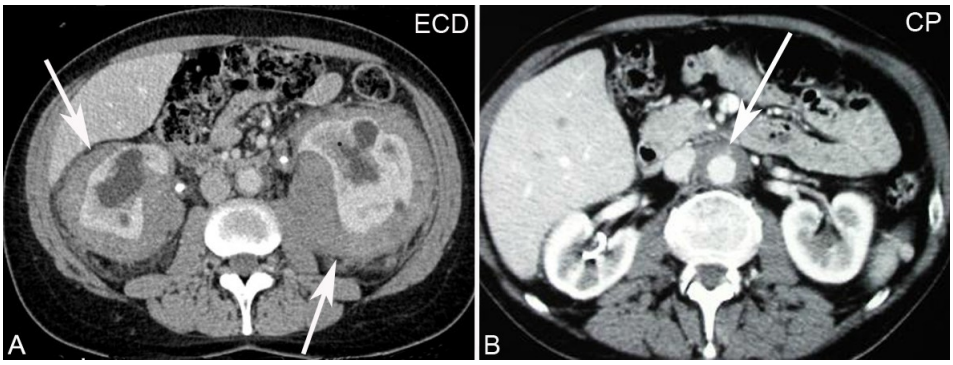

Figure 1. Contrast-enhanced abdominal computed tomography scan in a case of Erdheim-Chester disease (ECD) (A) and in a case of Chronic Periaortitis (CP) (B). The scan in A show the typical distribution of the pathologic tissue around the kidneys (arrows) that is seen in more than 50% of ECD patients. The scan in B shows the typical appearance of idiopathic periaortitis soft-tissue infiltration around the abdominal aorta (arrow)

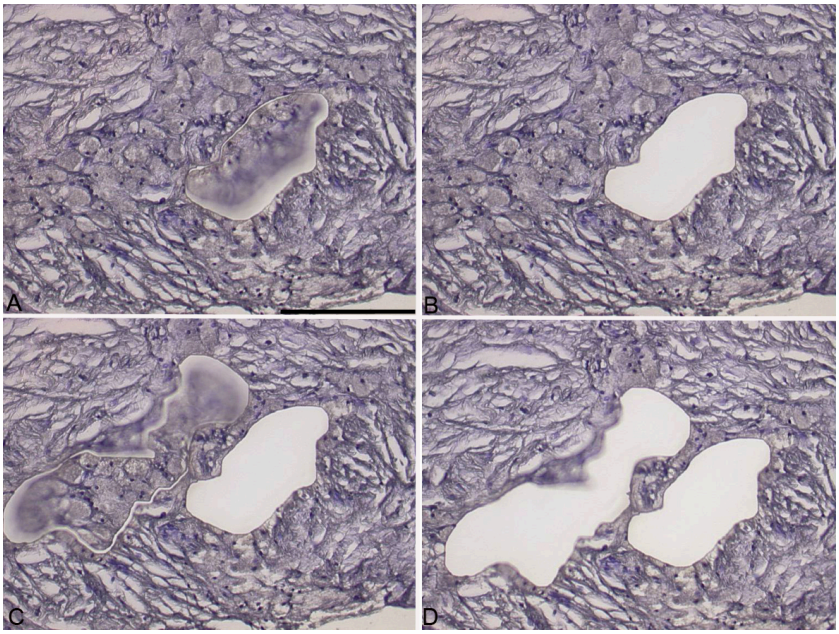

Figure 2. Pure histiocyte-rich areas obtained by laser capture microdissection. Original magnifications. A-D: x20 (bar is 150 μm.) Stainings. A-D: mildly counterstaining by Harris hematoxylin

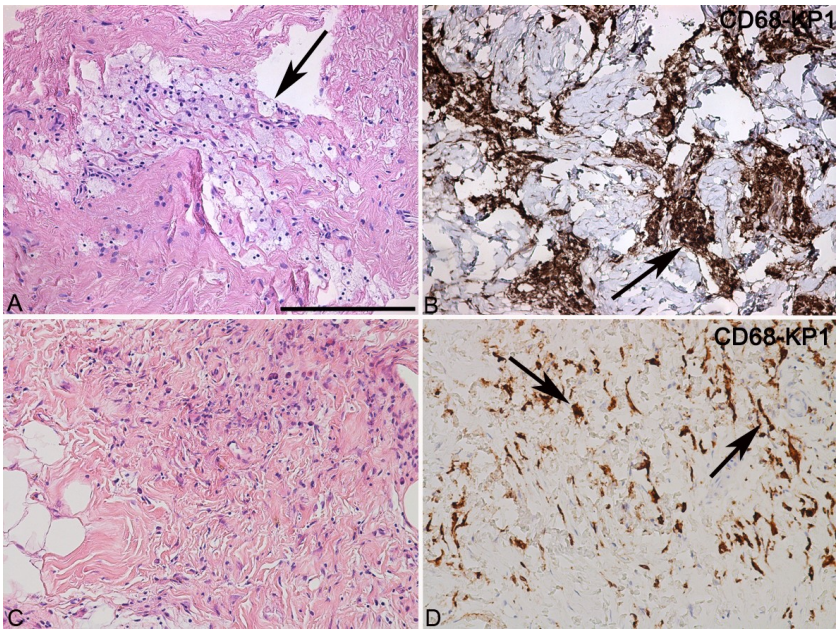

Figure 3. A. Medium-power view of an ECD histopathological field suitable for laser-capture microdissection. The arrow shows a homogeneous group of foamy histiocytes placed in scarcely cellular fibrous tissue. B. On immunohistochemistry, the CD68-KP1 decorates the cytoplasm of ECD histiocytes. C. Medium-power view of an ECD histopathological field non-suitable for laser-capture microdissection. The ECD histiocytes are dispersed into single, or small-group, elements which are better highlighted by an immunohistochemical analysis testing CD68-KP1 (arrows) (D). Original magnifications. A-D: x20 (bar is 150 µm). Stainings. A, C: hematoxylin-eosin. B, D: immunohistochemical analyses revealed by 3,3'-diaminobenzidine (DAB) and mildly counterstained by Harris hematoxylin

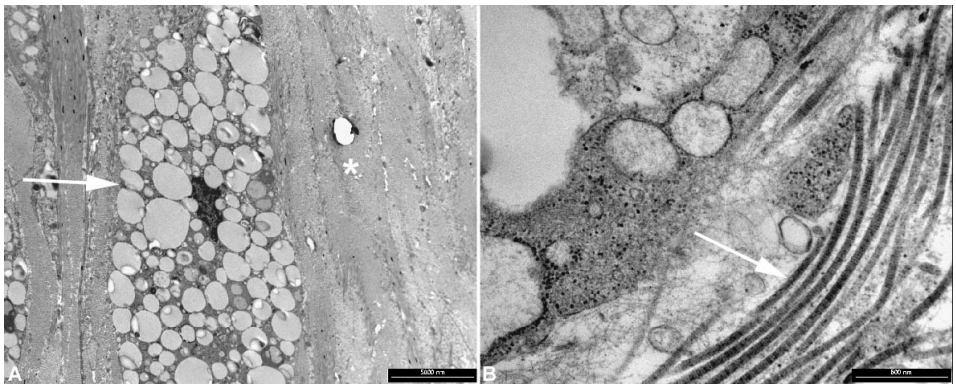

Figure 4. A. Low-power ultrastructural view of an ECD foamy histiocyte (arrow) placed in abundant collagen rich extracellular matrix (asterisk). B. At higher magnification, the same histiocyte shows aggregates of cytoplasmic thread-like fibrils with typical light and dark cross-striation in keeping with pro-collagen fibers (arrow). Original magnifications A: x28,000 (bar is 500 nm), B: x2,800 (bar is 5,000 nm)

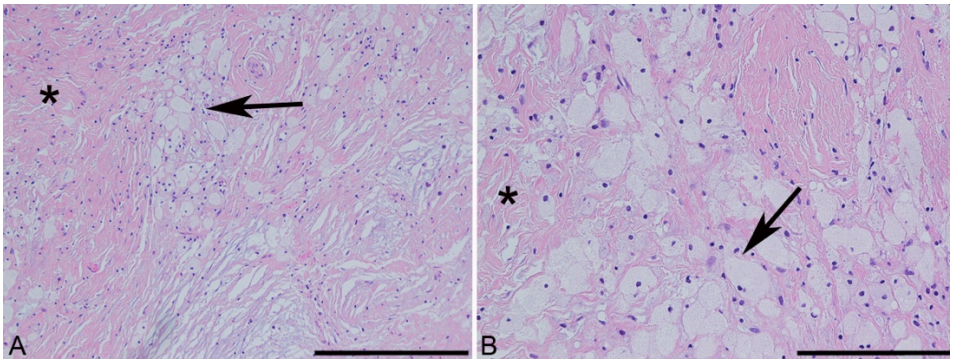

Figure 5. A. Low-power view of an ECD focus showing groups of histiocytes (arrow) within large amounts of fibrous tissue (asterisk). B. At higher magnification, these histiocytes (arrow) display clear-cut foamy appearance of their cytoplasms and a small round nucleus. Original magnifications. A: x10 (bar is 400 µm); B: x20 (bar is 150 µm). Stainings. A, B: hematoxylin-eosin

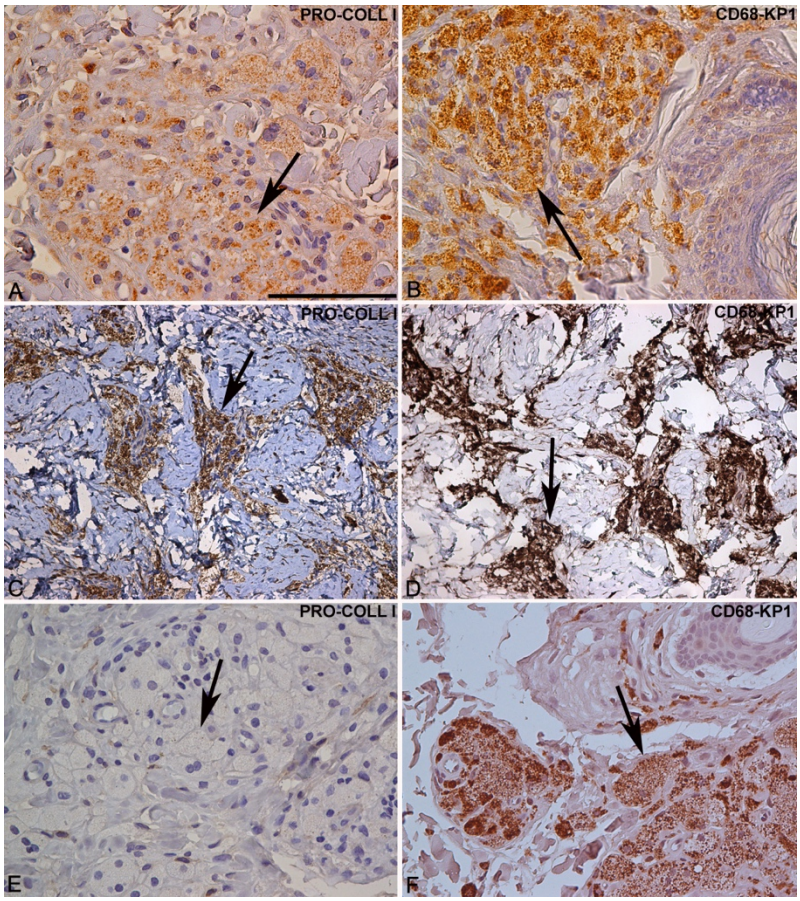

Figure 6. Pro-collagen type I (A and C) and CD68-KP1 (B and D) positivity in foamy histiocytes of skin and peri-renal biopsies from ECD patients. Pro-collagen type I negativity (E) and CD68-KP1 positivity (F) in foamy histiocytes of a non-ECD xanthoma. Original magnifications: A-F: x40 (bar is 100 µm). Stainings. A-D: immunohistochemical analyses revealed by 3,3'-diaminobenzidine (DAB) and mildly counterstained by Harris hematoxylin

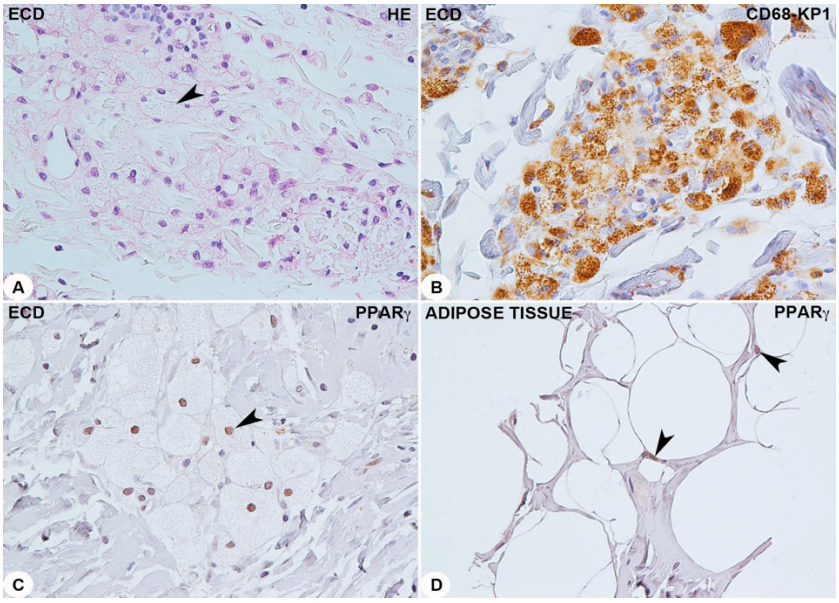

Figure 7. ECD histiocytes from a retroperitoneal biopsy showing typical foamy histiocytes (arrowhead) (A), these histiocytes are immunohistochemically positive for CD68- KP1 (B) and PPAR-γ antibodies (C, arrowhead). In the same biopsy, the nucleus of the resident adipose cells (arrowheads) stains with the same anti-PPAR-γ antibody (positive control). Original magnifications. A-D: x40 (bar is 100 µm). Stainings. A: hematoxylin-eosin. B-D: immunohistochemical analyses revealed by 3,3'-diaminobenzidine (DAB) and mildly counterstained by Harris hematoxylin

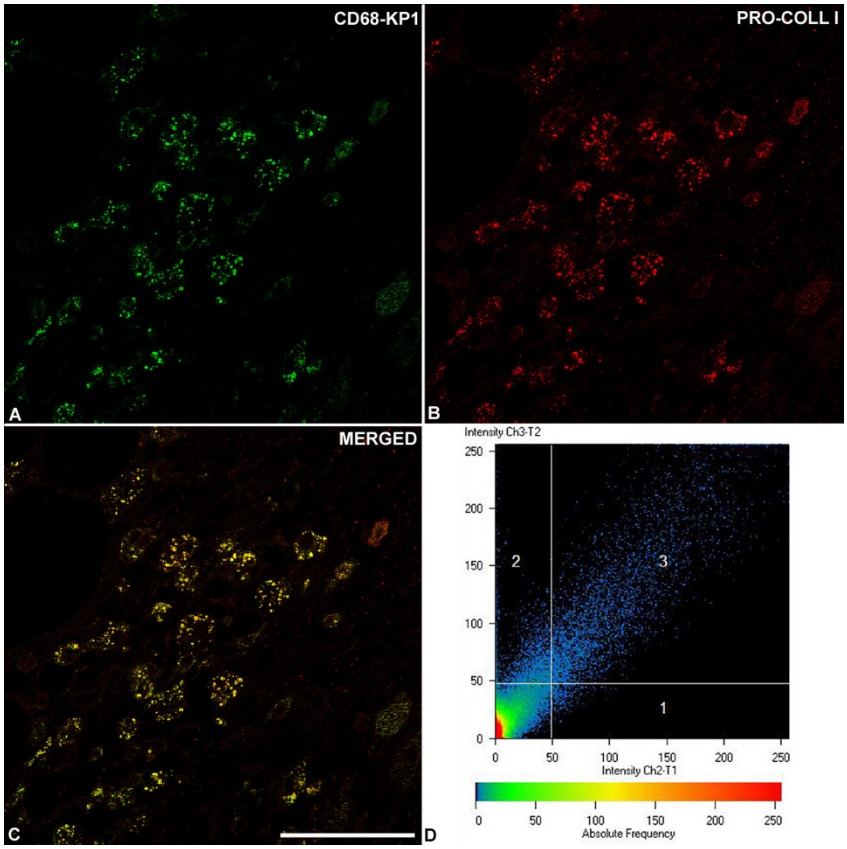

Figure 8. Confocal microscopy analysis simultaneously testing an anti-CD68-KP1 primary antibody (A) and an anti-pro-collagen I primary antibody (B) in a subcutaneous ECD location rich in foamy histiocytes. Image C shows the resulting merged image characterized by extreme superimposition of the green and red signals. D. Scatter plot for the analysis of colocalization showing a highly significant superimposition of the two single signals (green and red). All of the pixels of this image (this single confocal plane) are located in the four quadrants of the scatter graph with the background pixels within the bottom left quadrant. The single tagged pixels of the two channels are located in area 1 (green, CD68-KP1) and area 2 (red, pro-collagen I), while pixels having intensity above the background in both channels (colocalized pixels) are situated in the 3rd quadrant. Original magnifications: A, B, and C x63 (bar is 40 μm)

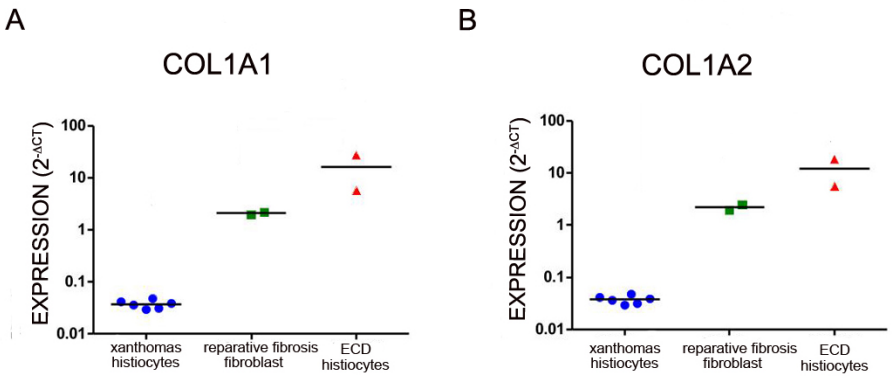

Figure 9. *COL1A1* (A) and *COL1A2* (B) genes are expressed in 2 ECD cases and in fibroblasts (used as positive controls) of 2 reparative fibroses while they are negative in 6 non-ECD xanthomas. The expression of the transcripts is calculated by $2^{-\Delta Ct}$. A-B: Real Time-PCR

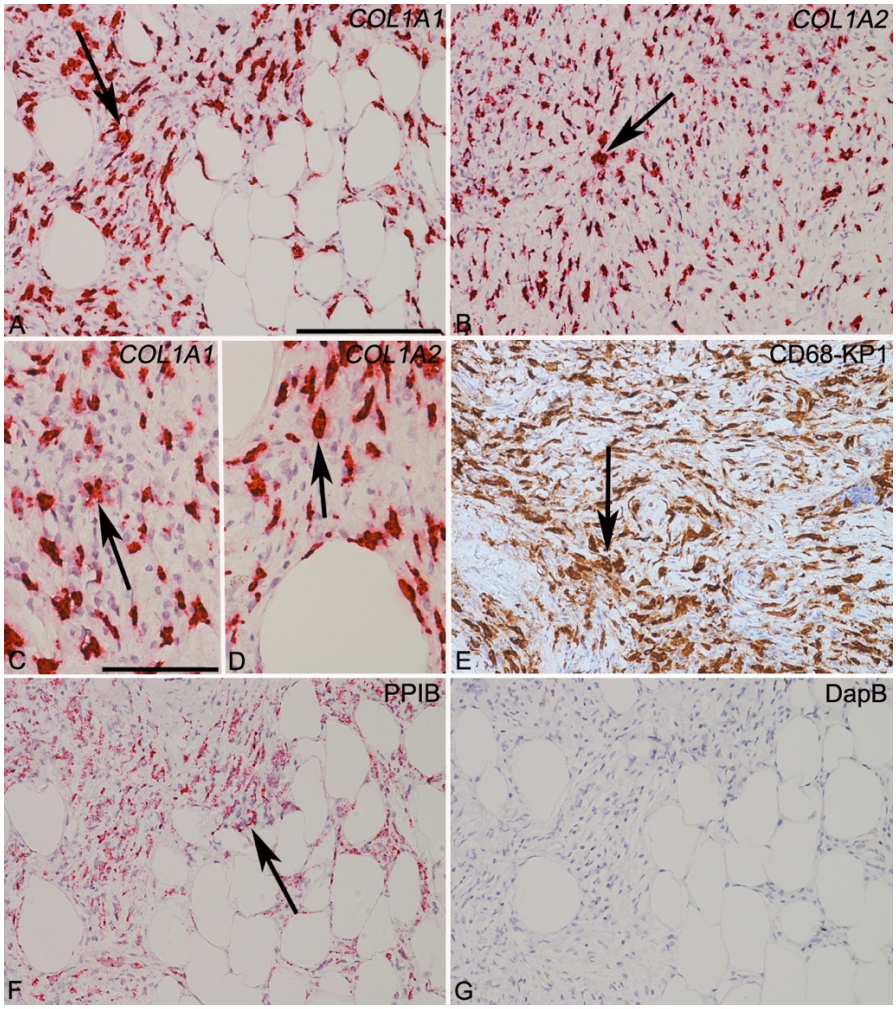

Figure 10. *COL1A1* and *COL1A2* genes in ECD histiocytes display significant gene expression in terms of reddish clusters (A-D). In the same ECD cases, the peptidylprolyl isomerase B (PPBI) – used as housekeeping gene – are expressed in small dots (F), while DapB (bacterial gene) – used as negative control probe – is negative (G). Original magnifications. A, B, E, F, G: x20 (bar is 150 μm); C, D x40 (bar is 100 μm). A-G: RNA in Situ Hybridization

Project 2 - Fibrocytes in Chronic Periaortitis. A novel mechanism linking inflammation and fibrosis

ABSTRACT

Objective. Chronic periaortitis (CP) is a rare disease characterised by a peri-aortic and peri-iliac fibro-inflammatory tissue. The pathogenic mechanisms leading to tissue accumulation and activation of fibroblasts are unclear. We explored the role of fibrocytes, circulating precursors of tissue fibroblasts, in patients with CP.

Methods. We studied 44 newly diagnosed CP patients and 30 healthy controls. Circulating fibrocytes were identified as collagen type I (Col I)$^+$/CD45$^+$ cells using flow cytometry; CP biopsies were stained with anti-pro-collagen-I (pro-col I), anti-CXCR4 and anti-CD45 antibodies and analysed by confocal microscopy to detect tissue-infiltrating fibrocytes. Circulating levels and tissue expression of CXCL12, a CXCR4 ligand that promotes fibrocyte homing, were investigated respectively using ELISA and immunohistochemistry. We also characterised T-helper (Th) polarisation in CP biopsies and measured serum levels of a panel of cytokines hallmarking Th responses and capable of influencing fibrocyte differentiation.

Results. The frequency of circulating Col I$^+$/CD45$^+$ fibrocytes was higher in patients than in controls (P=0.0371). CD45$^+$/pro-col I$^+$ and CXCR4$^+$/pro-col I$^+$ cells were detected in all examined CP biopsies. CXCL12 serum levels were also higher in CP patients (P=0.0056), and tissue-infiltrating inflammatory cells intensely expressed CXCL12. Increased serum levels of Th2-cytokines (*e.g.*, IL-13, IL-10) were found in patients, and immunohistochemistry revealed a dominant infiltration of GATA-3$^+$ cells, also indicating Th2-polarisation; Th2-skewed responses are known to promote fibrocyte differentiation.

Conclusions. Fibrocytes are enriched in the peripheral blood of CP patients and infiltrate target lesions; their accumulation in the pathologic tissue might be driven by CXCL12, and Th2-skewed immune responses are likely to facilitate their differentiation.

INTRODUCTION

Chronic periaortitis (CP) is a rare disease characterised by a periaortic fibro-inflammatory tissue that extends into the retroperitoneum and often causes ureteral obstruction. CP embraces idiopathic retroperitoneal fibrosis and inflammatory abdominal aortic aneurysms. Its pathogenesis is unclear: it is thought to be a manifestation of a systemic autoimmune disorder,[1] and in some cases it can be included in the spectrum of Immunoglobulin G4 (IgG4)-related disease (IgG4-RD).[2,3] The histological examination of CP biopsies shows the presence of two main components, an inflammatory infiltrate and a fibrous tissue. The inflammatory infiltrate comprises lymphocytes, macrophages, plasma cells and rare eosinophils, organised in two patterns, perivascular and diffuse. The fibrous component is rich in collagen type I as well as fibroblasts and myofibroblasts.[4,5] These cells are likely to determine tissue fibrosis but the pathogenic mechanisms leading to their accumulation and activation remain poorly understood. Fibrocytes are peripheral blood cells that originate from bone marrow progenitors. In the circulating blood, they account for less than 1% of total leukocytes. Fibrocytes have mixed leukocytic and mesenchymal features, and co-express CD45 (common leukocyte antigen), CD34 (hematopoietic stem cell antigen), markers of the monocyte lineage, and pro-collagen I (pro-col I) or collagen I (Col I); in their mature state, they constitutively express α-smooth muscle actin (αSMA).[6-11] Different factors promote differentiation and tissue recruitment of fibrocytes. T-helper (Th) 2 cytokines such as interleukin (IL)-4, IL-13, as well as transforming growth factor (TGF)-β1 promote fibrocyte differentiation, while Th1 cytokines such as interferon (IFN)-γ and tumour necrosis factor (TNF)-α have opposite effects.[12,13] Furthermore, fibrocytes exhibit cell surface chemokine receptors such as CXCR4, CCR7 and CCR3.[8,9,14] Several studies demonstrated that chemokine receptors are essential for the recruitment of

circulating fibrocytes to the sites of tissue damage, where they can promote fibrosis. In particular, stromal-derived factor-1 (SDF-1 or CXCL12), a ligand for CXCR4, is considered to be a crucial chemoattractant for fibrocytes to the sites of injury under inflammatory conditions.[15-18]

Fibrocytes participate in fibrosing and inflammatory diseases such as idiopathic pulmonary fibrosis, chronic asthma,[17-19] cardiovascular disease[16,20] and scleroderma.[13,21] Their role in the pathogenesis of CP or other IgG4-RD manifestations has never been investigated. In this study we explored the role of fibrocytes in CP; in particular, we assessed their frequency in the peripheral blood and their infiltration in CP lesions, along with the factors that may regulate this process.

METHODS

Patients

We included in this study 44 consecutive patients with newly diagnosed, clinically active, untreated CP and 30 age- and sex-matched healthy controls. The CP patients were diagnosed between 2013 and 2018. The diagnosis of CP was made based on commonly accepted radiological criteria.[3] In nine patients, retroperitoneal CP biopsy was also performed (via CT-guided, laparoscopic, or open procedures) to confirm the diagnosis. Causes of secondary retroperitoneal fibrosis (*e.g.*, infections, neoplasms, histiocytosis) were ruled out.[4] All patients underwent routine laboratory tests also including acute-phase reactants (erythrocyte sedimentation rate, ESR, and C-reactive protein, CRP), a panel of autoantibodies and IgG subclasses, as previously described.[2,3] They were all treated with conventional corticosteroid and/or immunosuppressive therapies.[2,3] Blood samples for serum collection and for isolation of peripheral blood mononuclear cells (PBMCs), were obtained at the time of diagnosis; the enrolled patients had to be untreated. The same samples were collected from 8 patients after 1 month of prednisone therapy and from one patient at the time of relapse. The study was conducted in accordance with the declaration of Helsinki and was approved by the local ethics committee.

Flow cytometric quantification of circulating fibrocytes

To perform flow cytometry analysis, we collected 36 mL of heparinised peripheral blood from 21 untreated patients at the time of enrolment, from 8 patients after 1 month of prednisone treatment, and from 1 patient at the time of relapse; the same amount of blood was also obtained from 24 control subjects. The PBMCs were isolated by Ficoll Hypaque

(Lympholyte, Cederlane Laboratories, Ontario, Canada) density gradient centrifugation, following the manufacturer's protocol. The cells were immediately used to identify circulating fibrocytes using a previously published protocol.[13] Briefly, 1.0 to 1.5x10^6 PBMCs/tube were suspended in 100µl of staining buffer and 5µl of FcR-blocking agent (Miltenyi, Bergisch Gladbach, Germany). The cells were stained with 20µl of PerCP-coniugated anti-CD45 antibody (BD Biosciences, San Jose, CA), washed and then fixed and permeabilised with the Cytofix/Cytoperm kit (BD Biosciences). After washing, the cells were incubated with 1µl of rabbit anti-human anti-Col I antibody (Rockland, Gilbertsville, PA) or 1µl of normal rabbit IgG, as isotype intracellular control antibody. After further washing, the cells were finally stained with 1µl of Alexa Fluor 610-R-PE goat anti-rabbit IgG secondary antibody (Invitrogen, Carlsband, CA). The samples were immediately acquired on a two-laser FACSCalibur cytometer (BD Biosciences) and between 0.5x10^6 and 0.7x10^6 events/tube were analysed using CELLQuest software. Live cells were selected based on FSC vs SSC plots, and the frequency of fibrocytes was defined as the percentage of anti-Col I^+ events within $CD45^+$ cells ($CD45^+$ Col I^+) after background subtraction (percentage of the events falling into the same region in the corresponding sample stained with isotype antibody). The median fluorescence intensity of anti-Col I (MFI Col I) was evaluated for each subject as MFI Col I minus MFI isotype control.

Tissue identification of fibrocytes and characterisation of lymphocyte infiltrates

Paraffin-embedded tissue samples from nine patients with CP were obtained from the files of the Unit of Pathology, Department of Medicine and Surgery, University of Parma. In order to confirm the original diagnosis, all histopathological slides were reviewed by an expert pathologist. The retroperitoneal biopsies used for this analysis had been fixed in a 10% buffered formalin solution, paraffin-embedded, and sectioned at 5µm. On these sections, we first

identified fibroblasts and myofibroblasts by immunohistochemistry using antibodies against vimentin (code MA5-11883, monoclonal, dilution 1:100; Invitrogen) and α-SMA (code ab124964, monoclonal, dilution 1:1000; Abcam, Cambridge, UK), and characterised the inflammatory infiltrate using antibodies against CD3 (code ab11089, monoclonal, dilution 1:250; Abcam), CD4 (code ab133616, monoclonal, dilution 1:200, Abcam), CD8 (code ab101500, monoclonal, dilution 1:150; Abcam), and CD20 (code ab9475, monoclonal, dilution 1:100; Abcam). We next investigated the presence of tissue-infiltrating fibrocytes with antibodies targeting CD45 (code ab40763, monoclonal, diluition 1:300; Abcam), CXCR4 (code PA3-305, polyclonal, dilution 1:200; Thermo Fischer Scientific), and pro-col I (code MAB1912, monoclonal, dilution 1:50; Millipore, Darmstadt, DE). Given that particular Th subsets are capable of influencing the differentiation of fibrocytes, we evaluated by immunohistochemistry the expression of the main transcription factors of Th1, Th2 and Th17 cells using antibodies respectively against T-bet (code ab91109, monoclonal, dilution 1:100; Abcam), GATA-3 (code abNBP1-47397, monoclonal, dilution 1:150; Novus Biologicals, Littleton, USA) and ROR-ɣt (code MABF81, monoclonal, 1:100; Millipore). All sections were counterstained with Harris' hematoxylin and examined with a bright light microscope (Nikon Eclipse 80i, Tokyo, JPN). The positivity of the Th cell subsets was evaluated using a semiquantitative method using a + to +++ grade scale (with + being 0-5%; ++ 5-20%, and +++ 20-100%) per microscopic field observed at a magnification of x 400.

We explored tissue expression of the CXCR4 ligand SDF-1 (CXCL12) with an anti-SDF-1 antibody (code ab18919, polyclonal, dilution 1:400; Abcam). All of the above reactions were revealed with 3,3′-diaminobenzidine, and the sections were counterstained with Harris' hematoxylin. The samples were examined with a bright light microscope (Nikon Eclipse 80i, Tokyo, JPN).

Tissue fibrocytes were further analysed by means of confocal microscopy analysis using an anti-pro-col I antibody in combination with anti-CD45 and anti-CXCR4 antibodies. The reaction of pro-col I was revealed by a tetramethylrhodamine probe (tetramethylrhodamine goat anti-rat IgG, code AP136R, dilution 1:70; Millipore) while the expression of CD45 and CXCR4 was revealed using a fluorescent probe (fluorescein isothiocyanate–conjugated goat anti-rabbit IgG, code AP187F, dilution 1:70; Millipore). The final immunofluorescence samples were observed under a confocal system (LSM 510 META scan head integrated with an Axiovert 200M inverted microscope; Carl Zeiss) with a x63 oil objective. The images were acquired in multitrack mode, using consecutive and independent optical pathways.

The immunohistochemistry and confocal microscopy methods were explained in detail in Project 1.

Cytokine and chemokine assessment

Six mL of serum were obtained from 24 patients at the time of enrolment (active disease, untreated). The same amount of serum was obtained from 14 control subjects. These samples were stored at -80°C until use. Before performing the assays described below, aliquots were thawed and centrifuged at 1,000g for 15 minutes at 4°C.

Using Bio-Rad Luminex assay technologies (Bio-Rad Laboratories, Life Science Group, Hercules, CA), we simultaneously analysed in 24 CP patients and 14 controls the levels of the following chemokines and cytokines which are able to influence fibrocyte differentiation: IL-4, IL-12, IFN-γ, IL-10, IL-13, IL-17, IL-1β, IL-8, interferon γ-induced protein (IP)-10, macrophage inflammatory protein (MIP)-1β, IL-9, and monocyte chemoattractant protein (MCP)-1. The assay was performed following the manufacturer's instructions. Briefly, samples diluted 1:2 with sample diluent were incubated for 2 hours with fluorescent beads coated with

the primary antibodies. All samples and standards were assayed in duplicate. Standard curves were generated by performing serial dilutions with a standard supplied in the kit. The wells were washed using a handheld magnetic washer and a biotinylated detector antibody was added for 1 hour. Then, the plates were washed and incubated for 30 minutes with streptavidin conjugated to the fluorescent protein R-phycoerythrin (Streptavidin-RPE). The beads were then washed to remove the unbound Streptavidin-RPE. The assay was analysed using a Luminex 100 instrument and the results examined using Bio-Rad Manager Software version 4.0.

We performed an ELISA (R&D Systems, Minneapolis, USA) to assess circulating levels of SDF-1 in the serum of 16 CP untreated patients, 8 CP treated patients and 10 healthy controls. The ELISA Kit was pre-coated with a monoclonal antibody directed towards human SDF-1. We placed into the wells 1:2 serial dilutions of standard and neat serum in duplicate and incubated for 2 hours at room temperature under shaking conditions. After washing, we added an enzyme-linked polyclonal antibody directed towards another epitope of human SDF-1 different from that recognised by the pre-coated monoclonal antibody. Following incubation and washing steps as previously described, we put the substrate solution into the wells and left them for 30 minutes at room temperature. We then added the stop solution and measured the optical density at 450nm and 550nm, using a microplate reader: subtraction of readings at 550nm from those at 450nm allows a correction for optical imperfections in the plate. A standard curve was produced by plotting the optical density of each standard on the y-axis against its concentrations on the x-axis, while SDF-1 concentration in our samples was measured through interpolation from the curve.

Statistical analysis

Continuous variables are presented as median (range or interquartile range) and categorical variables as n (%). Continuous variables were compared using the Mann Whitney U test for unpaired comparisons or the Wilcoxon test for paired comparisons. Correlations between clinical and laboratory parameters were assessed using Pearson's correlation analysis. P values <0.05 were considered statistically significant.

With regards to the comparisons in cytokine levels between CP patients and controls, considering that multiple cytokines were tested in the same experiment, the cut-off *P* value of 0.05 was corrected using Bonferroni's correction; the corrected cut-off *P* value (*P*corr) was therefore set at 0.0041.

RESULTS

The main demographic and clinical characteristics of the CP patients included in the study are reported in **table 1**.

Circulating fibrocytes

Circulating fibrocytes were enumerated in CP patients and healthy controls. Flow cytometry analysis showed that the proportion of fibrocytes, identified as $CD45^+$ Col I^+ cells, was higher in CP patients than in healthy controls. In particular, we found this double positive population in all of the 21 patients (100%) while only in 21 out 24 (87.5%) healthy controls; the median percentage of fibrocytes (defined as Col I^+ cells out of the total $CD45^+$ circulating cells) was 0.1% (range, 0.01–0.54%) in CP patients and 0.04% (range, 0-0.2%) in healthy controls (P=0.0371). These findings are shown in **figure 1**, where representative plots of fibrocyte flow cytometry staining in a CP patients and in a healthy controls are also included. The percentage of circulating fibrocytes did neither correlate with disease-related parameters such as CP thickness on CT/MRI, IgG4, ESR or CRP levels, nor with the degree of renal function impairment (data not shown). In eight patients PBMCs were available for fibrocytes evaluation also after the first month of prednisone treatment (1 mg/kg/day): the median fibrocyte percentage decreased from 0.085% (range, 0.03-0.54) to 0.04% (range, 0.01-0.08), although the difference did not reach statistical significance (P=0.09). In one patient with relapse, the median fibrocyte percentage was 0.11% at time of diagnosis, 0.04% after 1 month of treatment and returned to 0.11% at relapse (**figure 2**).

We also considered the levels of Col I expression within $CD45^+$ cells and found that patients' fibrocytes showed a higher intensity of Col I expression as compared with healthy controls'

fibrocytes (MFI Col I 313.72 versus 141.09; *P*=0.0459) (**figure 1**). Collectively, these results suggest that PBMCs from CP patients are enriched with $CD45^+$ Col I^+ cells.

Identification and characterisation of tissue fibrocytes

All of the nine CP biopsies showed the expected fibrous and inflammatory components.[5] In particular, the fibrous component was comprised of fibroblasts and myofibroblasts (characterised immunohistochemically as $vimentin^+$ and $\alpha\text{-}SMA^+$ cells, respectively) within varying amounts of collagen fibres (**figure 3**), while the inflammatory infiltrate was organised in two main patterns: perivascular and diffuse. The perivascular pattern consisted of lymphoid aggregates around small blood vessels; in some cases, these aggregates had the structure of secondary lymphoid follicles with a germinal centre and were characterised by $CD20^+$ B cells surrounded by $CD4^+$ and $CD8^+$ T lymphocytes (**figure 4**). The diffuse pattern consisted of sparse inflammatory infiltrates within the fibrous tissue, these infiltrates showing comparable amounts of $CD4^+$, $CD8^+$, and $CD20^+$ lymphocytes. In addition, the inflammatory component also included varying amounts of macrophages, plasma cells, and eosinophils (**figure 5**).

We next focused on the fibrous component and, in particular, on fibrocytes. The presence of these cells was explored by immunohistochemistry and confocal microscopy on the nine available CP biopsies. Using immunohistochemistry, we evaluated fibrocytes by testing the markers of these cells such as CD45, pro-col I, and CXCR4. Because the fibrocyte immunophenotype is characterised by specific combinations of the above markers, we identified these tissue-infiltrating cells by evaluating the co-expression of pro-col I with either CD45 or CXCR4 by using confocal microscopy. Overall, $CD45^+$ pro-col I^+ and $CXCR4^+$ pro-col I+ spindle-shaped cells were found in all the examined biopsies (**figure 6**) and their density respectively ranged from 2 to 6 cells and from 4 to 8 cells per mm^2 of tissue.

Tissue recruitment of fibrocytes and factors influencing their differentiation

The tissue expression of SDF-1/CXCL12 (the ligand of CXCR4) in CP biopsies was analysed to investigate whether this chemokine is potentially involved in fibrocyte recruitment. We assessed SDF-1 expression by immunohistochemistry in the nine available CP biopsies, where this protein showed a strong immunosignal in both inflammatory cells and fibroblasts (**figure 7**).

Next, we determined SDF-1 serum concentrations by ELISA in 16 CP untreated patients, 10 healthy controls and in 8 prednisone-treated patients. SDF-1 serum concentrations were significantly higher in CP patients than in the controls [median, 3064 pg/ml (range, 2139-4679) vs. 2516 pg/ml (range 2164-2839), respectively; P=0.0056]. Subsequently, we analysed serum SDF-1 concentrations in 8 untreated patients and in the same patients after 1 month of prednisone therapy. We observed a post-treatment reduction in SDF-1 serum levels which reached statistical significance [median, 3019 pg/ml (range, 2139-3879) vs. 2131.5 pg/ml (range 1724-2889), respectively; P=0.02] (**figure 7**).

The SDF-1 levels of the untreated patients correlated positively with ESR (=0.55; P=0.02) and negatively with Hb (=-0.64; P=0.009). No correlation was found between serum SDF-1 levels and concentrations of peripheral fibrocytes (data not shown). Also, no correlations or associations were found between SDF-1 and other laboratory parameters (*e.g.*, serum IgG4, creatinine, CRP) or with disease-related characteristics (*e.g.*, non-aneurysmal vs. aneurysmal CP, CP localisation, hydronephrosis) (data not shown).

The differentiation of fibrocytes can be influenced by the inflammatory milieu, and the polarisation of Th immune responses seems to play a major role in this respect. We therefore examined the Th polarisation of tissue-infiltrating $CD4^+$ T cells by immunohistochemistry by staining for their main transcription factors.

Immunohistochemical analysis showed – albeit with quantitative differences from case to case – a predominance of GATA-3^+ and, to a lesser extent, of T-bet^+ cells. Of the nine biopsies analysed, none showed 1^+, eight showed 2^+ and one 3^+ T-bet^+ cells, whereas with respect to GATA-3^+ cells the biopsies showed 1^+ in one case, 2^+ in four and 3^+ in four. The extent of RORγt^+ cell infiltration was consistently $1^+/2^+$ (**figure 8**).

We next tested the serum levels of an array of cytokines potentially influencing Th polarisation and, consequently, fibrocyte differentiation. The serum levels of several cytokines were higher in CP patients than in the controls, but those that reached statistical significance (*P* values below *P*corr cut-off of 0.0041) were only IL-9 (*P*=0.0016), IL-10 (*P*=0.0032), IL-12 (*P*=0.0011), and IL-13 (*P*=0.0004) (**figure 8 and figure 9**).

DISCUSSION

CP is a rare idiopathic disease hallmarked by exuberant fibrosis and a chronic inflammatory infiltrate, typically localised in the retroperitoneal space surrounding the abdominal aorta and the iliac arteries. CP is part of the spectrum of IgG4-RD together with other fibro-inflammatory conditions such as sclerosing pancreato-cholangitis, fibrosing mediastinitis, Mikulicz's disease and inflammatory pseudotumours, but the proportion of CP cases that can be labelled as IgG4-related is still unclear.[2] While recent studies have characterised the inflammatory infiltrate found in CP and some of the cytokines and chemokines (*e.g.*, IL-6, eotaxin/CCL11) involved in this process,[22,23] the mechanisms that drive the aberrant fibrous response have never been investigated. The present study demonstrates that fibrocytes, precursors of tissue fibroblasts, are enriched in the circulation of CP patients and infiltrate target lesions; we also found increased serum levels and intense tissue expression of CXCL12/SDF-1, a chemokine that is able to drive their accumulation in the pathologic lesions. Finally, we also detected in CP biopsies a Th2-skewed immune response, which probably facilitates fibrocyte differentiation.

Bloodborne fibrocytes were first identified in a murine model of skin wound repair and in human wounded skin as $CD34^+$ spindle-shaped cells.[24] Subsequent studies showed that they originate from monocyte precursors, express leukocyte markers (*e.g.*, CD45) and fibroblast proteins (*e.g.*, vimentin), and have the ability to produce different types of collagen as well as other extracellular matrix proteins. Additionally, since their migration into the diseased sites is regulated by specific chemokines, they also express chemokine receptors such as CXCR4.[25] Fibrocytes participate in the normal response to acute tissue injury and contribute to tissue repair; they have multiple functional properties, being not only pro-fibrotic but also capable of

modulating angiogenesis and both innate and adaptive immune responses.[26,27] Recently, it has become clear that they are also involved in human disease, particularly in conditions characterised by chronic inflammation, excessive extracellular matrix production and tissue remodelling, examples of which include asthma, chronic lung disease (*e.g.*, idiopathic pulmonary fibrosis), autoimmune (*e.g.*, systemic sclerosis, rheumatoid arthritis) and cardiovascular diseases.[6,28,29] In most of these diseases, both the circulating and tissue fibrocyte compartments are expanded: elevated numbers of fibrocytes were detected in rheumatoid arthritis, Graves' ophthalmopathy, idiopathic pulmonary fibrosis as well as in murine models of collagen-induced arthritis. Notably, the frequency of peripheral blood fibrocytes has been validated as a prognostic marker in pulmonary fibrosis.[30] Intense tissue infiltration by fibrocytes was found particularly in the subepithelial airway mucosa of patients with chronic asthma, where such cells synthesise Col I, express α-SMA and localise to areas of extracellular matrix deposition.[31,32]

We found an increased frequency of circulating fibrocytes (identified as $CD45^+$ Col I^+ cells) in patients with active, untreated CP as compared with healthy controls, although we could not demonstrate correlations or associations with disease-related parameters (*e.g.*, acute-phase reactants), clinical manifestations or specific disease phenotypes such as IgG4-related cases. The peripheral fibrocyte concentrations observed in our study subjects are in the range of those reported in other conditions, although the results are often difficult to compare due to heterogeneous staining or isolation techniques.[19,28] Remarkably, we also detected significant amounts of fibrocytes in CP biopsies, where such cells were identified not only on the basis of their dual positivity for CD45 and pro-col I but also as pro-col I^+ cells co-expressing CXCR4, the receptor of CXCL12/SDF-1, a chemokine that regulates fibrocyte homing.[21,32,33] In line with this observation, we also demonstrated that serum levels of CXCL12/SDF-1 were

increased in patients with active CP and that, at the tissue level, this chemokine was intensely expressed by mononuclear cells constituting the lymphoid aggregates. Of note, we observed that serum levels of CXCL12/SDF-1 declined in the 8 treated CP patients. $CXCR4^+$ tissue fibrocytes were revealed in autoimmune diseases such as Graves' ophthalmopathy;[34] notably, the CXCR4-CXCL12 axis was shown to be a major determinant of fibrocyte tissue recruitment in murine models of bleomycin-induced lung fibrosis, and therapeutic inhibition of this axis reduced the magnitude of fibrosis.[33] Collectively, these data suggest that the CXCR4-CXCL12 axis operates in CP and may contribute to tissue recruitment of fibrocytes.

Other chemokines are involved in fibrocyte homing; one example is eotaxin/CCL11, a chemokine usually produced in response to Th2-responses.[35] Through ligation of CCR3, eotaxin/CCL11 mediates tissue influx of several cell types including eosinophils and mast cells. In a previous study, we showed that the serum levels of eotaxin/CCL11 are increased in active CP, that it is produced by mononuclear inflammatory cells, and that in CP lesions its receptor CCR3 is intensely expressed by several cell types including fibroblasts.[22]

Fibrocytes play a role in conditions that are histologically characterised by monocyte– and T cell-rich inflammation, and their proliferation is influenced by specific T-cell responses. In particular, fibrocyte expansion appears to be enhanced by Th2 cytokines such as IL-4 and IL-13 and inhibited by Th1- or Th17-related cytokines such as IFN-γ and IL-17.[36] We characterised Th polarisation in CP by testing circulating levels of cytokines associated with distinct Th responses, and also by analysing the tissue expression of transcription factors such as T-bet, GATA-3 and RORγt, that respectively hallmark Th1, Th2, and Th17 cells. We found a strong Th2 signal, based on the marked increase in Th2 cytokines in the serum, namely IL-13 and IL-10, and the intense expression of GATA-3 in CP biopsies. We also detected a significant increase in IL-12, usually associated with Th1-responses, but tissue expression of the Th1

marker T-bet was less abundant than that of GATA-3. On the other hand, serum IL-17 was not increased, and tissue expression of RORγt was low. Taken together, these findings indicate that Th responses in CP are mainly polarised towards a Th2 phenotype, which might be a driver of fibrocyte expansion in the circulation and of its differentiation in the affected tissues. The functional implication of the observed increase in serum IL-9 is difficult to interpret, although this pleotropic cytokine has also been associated with Th2, allergic and chronic inflammatory reactions.[37]

Once fibrocytes infiltrate target tissues, they not only differentiate into fibroblasts and myofibroblasts, thus promoting fibrosis, but may also have pro-inflammatory effects.[38] This could amplify the inflammatory response and contribute to the parallel development of inflammation and fibrosis that is seen in the early stages of CP. In keeping with this view, we previously showed that the pro-inflammatory cytokine IL-6 is also intensely expressed by fibroblasts in CP lesions.[23]

In conclusion, fibrocytes are likely to play a role in the pathogenesis of CP; they are increased in the circulation of patients with active disease and infiltrate target lesions. Their tissue recruitment can be driven by chemokines such as SDF-1, and Th2-skewed immune responses can contribute to their expansion.

Most of this data has been published in *Arthritis & Rheumatology* (IF: 9.002)

Maria Nicastro, B.Sc, Rosanna Vescovini, PhD, Federica Maritati, MD, Alessandra Palmisano, MD, Maria L. Urban, MD, Monia Incerti, B.Sc, Paride Fenaroli, MD, Francesco Peyronel, MD, Giuseppe D. Benigno, MD, Domenica Mangieri, PhD, Riccardo Volpi, MD, Gabriella Becchi, Paola Romagnani, MD PhD, Domenico Corradi, MD, and Augusto Vaglio, MD, PhD.

REFERENCES

1. Martorana D, Marquez A, Carmona FD, et al. A large-scale genetic analysis reveals an autoimmune origin of idiopathic retroperitoneal fibrosis. J Allergy Clin Immunol 2018; 142(5): 1662-5.
2. Rossi GM, Rocco R, Accorsi Buttini E, Marvisi C, Vaglio A. Idiopathic retroperitoneal fibrosis and its overlap with IgG4-related disease. Intern Emerg Med 2017; 12(3): 287-99.
3. Vaglio A, Maritati F. Idiopathic Retroperitoneal Fibrosis. J Am Soc Nephrol 2016; 27(7): 1880-9.
4. Urban ML, Palmisano A, Nicastro M, Corradi D, Buzio C, Vaglio A. Idiopathic and secondary forms of retroperitoneal fibrosis: a diagnostic approach. Rev Med Interne 2015; 36(1): 15-21.
5. Corradi D, Maestri R, Palmisano A, et al. Idiopathic retroperitoneal fibrosis: clinicopathologic features and differential diagnosis. Kidney Int 2007; 72(6): 742-53.
6. Bellini A, Mattoli S. The role of the fibrocyte, a bone marrow-derived mesenchymal progenitor, in reactive and reparative fibroses. Lab Invest 2007; 87(9): 858-70.
7. Bucala R. Fibrocytes at 20 Years. Mol Med 2015; 21 Suppl 1: S3-5.
8. Cao T, Rajasingh S, Rajasingh J. Circulating fibrocytes serve as a marker for clinical diagnosis. Ann Transl Med 2016; 4(Suppl 1): S38.
9. Sakai N, Wada T, Yokoyama H, et al. Secondary lymphoid tissue chemokine (SLC/CCL21)/CCR7 signaling regulates fibrocytes in renal fibrosis. Proc Natl Acad Sci U S A 2006; 103(38): 14098-103.
10. Pilling D, Fan T, Huang D, Kaul B, Gomer RH. Identification of markers that distinguish monocyte-derived fibrocytes from monocytes, macrophages, and fibroblasts. PLoS One 2009; 4(10): e7475.
11. Just SA, Lindegaard H, Hejbol EK, et al. Fibrocyte measurement in peripheral blood correlates with number of cultured mature fibrocytes in vitro and is a potential biomarker for interstitial lung disease in Rheumatoid Arthritis. Respir Res 2017; 18(1): 141.
12. Shao DD, Suresh R, Vakil V, Gomer RH, Pilling D. Pivotal Advance: Th-1 cytokines inhibit, and Th-2 cytokines promote fibrocyte differentiation. J Leukoc Biol 2008; 83(6): 1323-33.
13. Russell TM, Herzog EL, Bucala R. Flow cytometric identification of fibrocytes in scleroderma lung disease. Methods Mol Biol 2012; 900: 327-46.
14. Mack M. Inflammation and fibrosis. Matrix Biol 2018; 68-69:106-21.
15. Herzog EL, Bucala R. Fibrocytes in health and disease. Exp Hematol 2010; 38(7): 548-56.
16. Lei PP, Qu YQ, Shuai Q, et al. Fibrocytes are associated with the fibrosis of coronary heart disease. Pathol Res Pract 2013; 209(1): 36-43.
17. Andersson-Sjoland A, de Alba CG, Nihlberg K, et al. Fibrocytes are a potential source of lung fibroblasts in idiopathic pulmonary fibrosis. Int J Biochem Cell Biol 2008; 40(10): 2129-40.
18. Mehrad B, Burdick MD, Zisman DA, Keane MP, Belperio JA, Strieter RM. Circulating peripheral blood fibrocytes in human fibrotic interstitial lung disease. Biochem Biophys Res Commun 2007; 353(1): 104-8.
19. Dupin I, Allard B, Ozier A, et al. Blood fibrocytes are recruited during acute exacerbations of chronic obstructive pulmonary disease through a CXCR4-dependent pathway. J Allergy Clin Immunol 2016; 137(4): 1036-42 e7.

20. Keeley EC, Mehrad B, Strieter RM. The role of fibrocytes in fibrotic diseases of the lungs and heart. Fibrogenesis Tissue Repair 2011; 4: 2.
21. Reilkoff RA, Bucala R, Herzog EL. Fibrocytes: emerging effector cells in chronic inflammation. Nat Rev Immunol 2011; 11(6): 427-35.
22. Mangieri D, Corradi D, Martorana D, et al. Eotaxin/CCL11 in idiopathic retroperitoneal fibrosis. Nephrol Dial Transplant 2012; 27(10): 3875-84.
23. Vaglio A, Catanoso MG, Spaggiari L, et al. Interleukin-6 as an inflammatory mediator and target of therapy in chronic periaortitis. Arthritis Rheum 2013; 65(9): 2469-75.
24. Bucala R, Spiegel LA, Chesney J, Hogan M, Cerami A. Circulating fibrocytes define a new leukocyte subpopulation that mediates tissue repair. Mol Med 1994; 1(1): 71-81.
25. Mattoli S. Involvement of fibrocytes in asthma and clinical implications. Clin Exp Allergy 2015; 45(10): 1497-509.
26. Chesney J, Bacher M, Bender A, Bucala R. The peripheral blood fibrocyte is a potent antigen-presenting cell capable of priming naive T cells in situ. Proc Natl Acad Sci U S A 1997; 94(12): 6307-12.
27. Hartlapp I, Abe R, Saeed RW, et al. Fibrocytes induce an angiogenic phenotype in cultured endothelial cells and promote angiogenesis in vivo. FASEB J 2001; 15(12): 2215-24.
28. Galligan CL, Siminovitch KA, Keystone EC, Bykerk V, Perez OD, Fish EN. Fibrocyte activation in rheumatoid arthritis. Rheumatology (Oxford) 2010; 49(4): 640-51.
29. Peng H, Herzog EL. Fibrocytes: emerging effector cells in chronic inflammation. Curr Opin Pharmacol 2012; 12(4): 491-6.
30. Moeller A, Gilpin SE, Ask K, et al. Circulating fibrocytes are an indicator of poor prognosis in idiopathic pulmonary fibrosis. Am J Respir Crit Care Med 2009; 179(7): 588-94.
31. Nihlberg K, Larsen K, Hultgardh-Nilsson A, Malmstrom A, Bjermer L, Westergren-Thorsson G. Tissue fibrocytes in patients with mild asthma: a possible link to thickness of reticular basement membrane? Respir Res 2006; 7: 50.
32. Saunders R, Siddiqui S, Kaur D, et al. Fibrocyte localization to the airway smooth muscle is a feature of asthma. J Allergy Clin Immunol 2009; 123(2): 376-84.
33. Mehrad B, Burdick MD, Strieter RM. Fibrocyte CXCR4 regulation as a therapeutic target in pulmonary fibrosis. Int J Biochem Cell Biol 2009; 41(8-9): 1708-18.
34. Douglas RS, Afifiyan NF, Hwang CJ, et al. Increased generation of fibrocytes in thyroid-associated ophthalmopathy. J Clin Endocrinol Metab 2010; 95(1): 430-8.
35. Dorman SC, Babirad I, Post J, et al. Progenitor egress from the bone marrow after allergen challenge: role of stromal cell-derived factor 1alpha and eotaxin. J Allergy Clin Immunol 2005; 115(3): 501-7.
36. Bellini A, Marini MA, Bianchetti L, Barczyk M, Schmidt M, Mattoli S. Interleukin (IL)-4, IL-13, and IL-17A differentially affect the profibrotic and proinflammatory functions of fibrocytes from asthmatic patients. Mucosal Immunol 2012; 5(2): 140-9.
37. Ciccia F, Guggino G, Ferrante A, Cipriani P, Giacomelli R, Triolo G. Interleukin-9 and T helper type 9 cells in rheumatic diseases. Clin Exp Immunol 2016; 185(2): 125-32.
38. Chesney J, Metz C, Stavitsky AB, Bacher M, Bucala R. Regulated production of type I collagen and inflammatory cytokines by peripheral blood fibrocytes. J Immunol 1998; 160(1): 419-25.

Table

Table 1. Demographic and clinical characteristics of the Chronic Periaortitis (CP) patients included in the study

	CP patients N=44
Age, years – *median (IQR)*	57.5 (52.8–63.5)
Male gender, *n (%)*	28 (63.6)
Peri-aneurysmal/non-aneurysmal CP, n	5/39
Clinical manifestations, n (%)	
Constitutional symptoms	31 (70.4)
Abdominal/lumbar pain	38 (86.4)
Deep vein thrombosis	5 (11.4)
Hydronephrosis	29 (65.9)
Unilateral	12 (27.3)
Bilateral	17 (38.6)
Acute renal failure	17 (38.6)
Extra-retroperitoneal fibro-inflammatory lesions[§]	5 (11.4)
Laboratory markers	
ESR, mm/h – *median (IQR)*	62 (46.5–90.5)
CRP, mg/L– *median (IQR)*	25.5 (11.7–40.5)
WBC, x 10^{9}/uL– *median (IQR)*	6.8 (6.1–7.5)
Haemoglobin, g/dL– *median (IQR)*	11.8 (10.9–13.2)
Creatinine, mg/dL– *median (IQR)*	1.3 (0.9–2.9)
ANA positivity, *n (%)*	13 (29.5)
IgG4, mg/dL – *median (IQR)*	70.5 (33–141.5)
Comorbidity, n (%)	
Cardiovascular disease*	6 (13.6)
Autoimmune disease	17 (38.6)
Autoimmune thyroiditis	10 (22.7)
Other autoimmune diseases	9 (20.5)

[§]Extra-retroperitoneal fibro-inflammatory lesions include thoracic periaortitis, fibrosing mediastinitis, tubulo-interstitial nephritis w/wo membranous nephropathy, chronic sclerosing pancreato-cholangitis, orbital pseudotumour, lung pseudotumour

*Cardiovascular disease denotes clinically overt ischemic heart disease, cerebrovascular disease and peripheral arterial disease

Figures

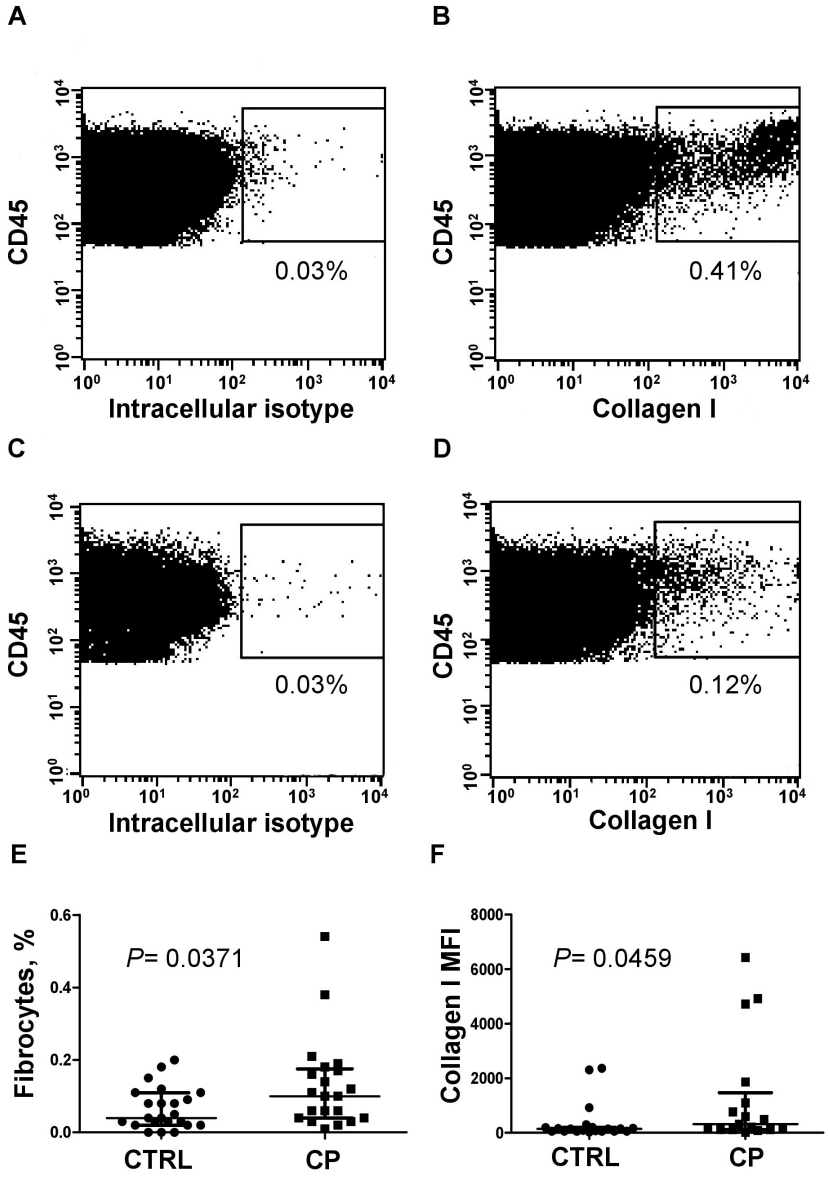

Figure 1. Flow cytometric identification of fibrocytes in the peripheral blood of chronic periaortitis (CP) patients. Representative plots of flow cytometry analysis in a CP patient (A and B) and a healthy control (C and D). PBMCs were stained as described in the Methods section. Live mononuclear cells were selected based on CD45 vs. SSC plot (not shown) and fibrocytes were defined as the percentage of anti-collagen type I positive events within CD45 positive cells (gates in B and D), minus the percentage of the events falling into the same region with isotype antibody (gates in A and C, respectively). E. Comparison of fibrocyte frequencies between CP patients and healthy controls. F. Comparison of the median fluorescence intensity (MFI) of anti-collagen type I expressed by fibrocytes from patients and from controls. In each scatter plot, median (bar) and interquartile range are shown. The Mann-Whitney non-parametric test was used for statistical analysis

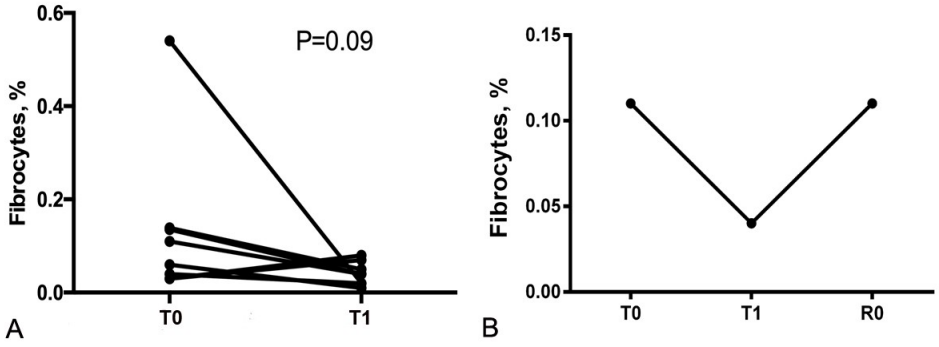

Figure 2. A. Circulating fibrocyte percentages in eight patients before (T0) and after one month of prednisone therapy (T1). The difference between the two time-points was assessed using Wilcoxon test for paired data. B. In only 1 case with relapse, were circulating fibrocyte percentages higher at time of diagnosis (T0), lower after 1 month of treatment (T1), and higher again during recurrence (R0)

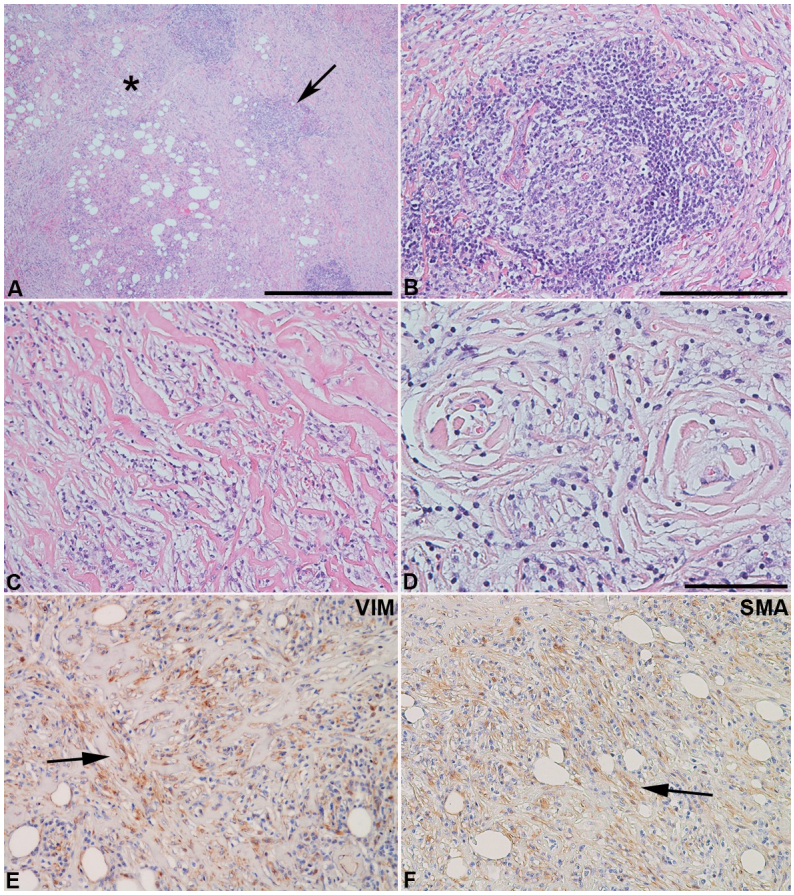

Figure 3. A. Low-power histopathological view of a CP biopsy characterised by fibrous replacement of the retroperitoneal soft tissues with chronic inflammatory infiltrates which are organised into nodular aggregates (arrow) and a diffuse pattern between the thick collagen fibres (asterisk). Sparse residual adipose tissue areas can be found. B. At higher magnification, it can be noted that the nodular inflammatory aggregates are organised around small blood vessels; hence, the designation of “perivascular pattern”. C. The diffuse inflammatory pattern consists of inflammatory elements distributed between thick collagen fibres. D. Collagen fibres are typically arranged around the adventitia of small vessels with an "onion bulb" appearance. Among the collagen fibres, there are lymphocytes, plasma cells, histiocytes, fibroblasts/myofibroblasts, and rare eosinophils. Fibroblasts/myofibroblasts show immunohistochemical positivity for vimentin (E) and smooth muscle actin (F). Original magnifications. A: x4 (bar is 1mm); B, C, E, F: x20 (bar is 150 µm); D: x40 (bar is 100 µm). Stainings. A-D: hematoxylin-eosin. E-F: immunohistochemical analyses revealed by 3,3'-diaminobenzidine (DAB) and mildly counterstained by Harris hematoxylin

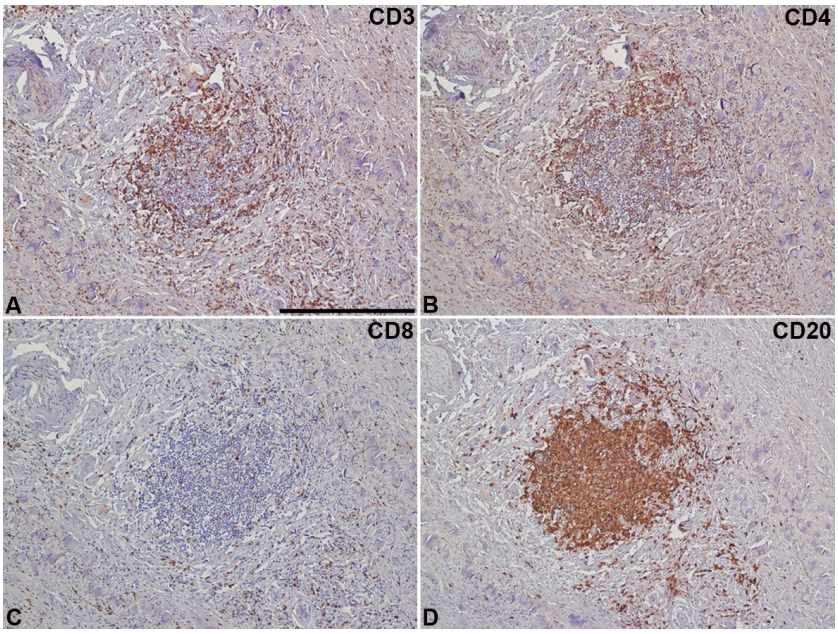

Figure 4. Perivascular lymphocyte aggregates consist of a periphery of $CD3^+$ T lymphocytes (A) and a dense core of $CD20^+$ B lymphocytes (D). The T lymphocyte component is characterised primarily by $CD4^+$ cells (B), whereas $CD8^+$ cells represent only a minority (C). Original magnification. A-D: x10 (bar is 400 um) Stainings. A-D: immunohistochemical analyses revealed by 3,3'-diaminobenzidine (DAB) and mildly counterstained by Harris hematoxylin

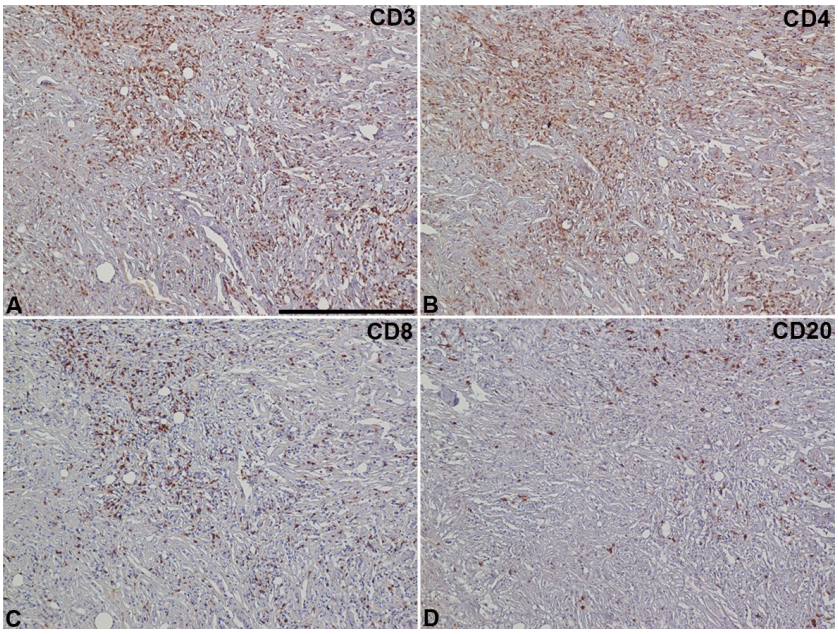

Figure 5. The diffuse lymphocyte infiltrate mainly consists of $CD3^+$ T lymphocytes (A) and a minority of $CD20^+$ B lymphocytes (D). The T cell component includes both $CD4^+$ (B) and $CD8^+$ (C) cells. Original magnification. A-D: x10 (bar is 400 µm) Stainings: immunohistochemical analyses revealed by 3,3'-diaminobenzidine (DAB) and mildly counterstained by Harris hematoxylin

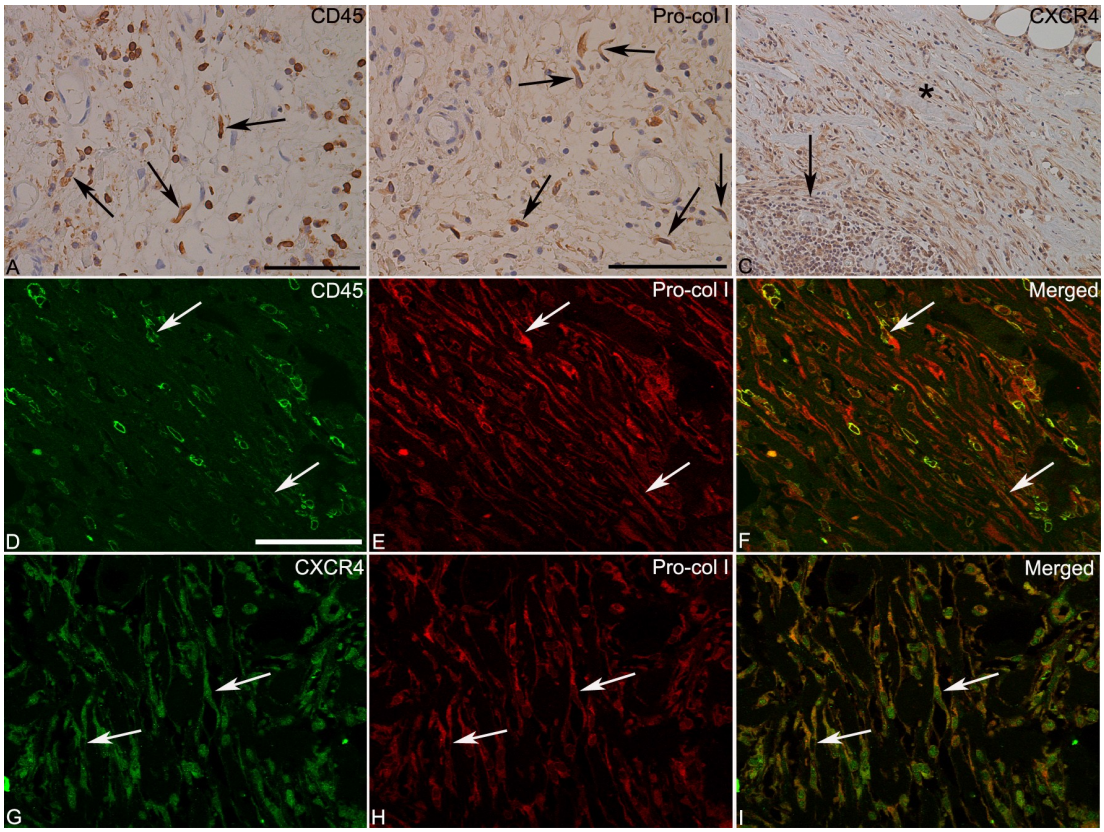

Figure 6. Fibrocytes in CP biopsies. An immunohistochemical analysis reveals the presence of spindled elements (arrows) positive for CD45 (A), pro-collagen type I (B), and CXCR4 (C). The co-expression of pairs of the above markers in these elongated cells (arrows) has been demonstrated by confocal microscopy by contemporarily testing CD45/pro-collagen type I (D), E, and F) and CXCR4/pro-collagen type I (G, H, and I). These co-expressions identify these cells as fibrocytes. Original magnifications. A and B: x40 (bar is 100 µm); C: x20 (bar is 150 µm); D-I: x63 (bar is 40 µm). Stainings. A-C: immunohistochemical analyses revealed by 3,3'-diaminobenzidine (DAB) and mildly counterstained by Harris hematoxylin; D-I: immunofluorescence analyses

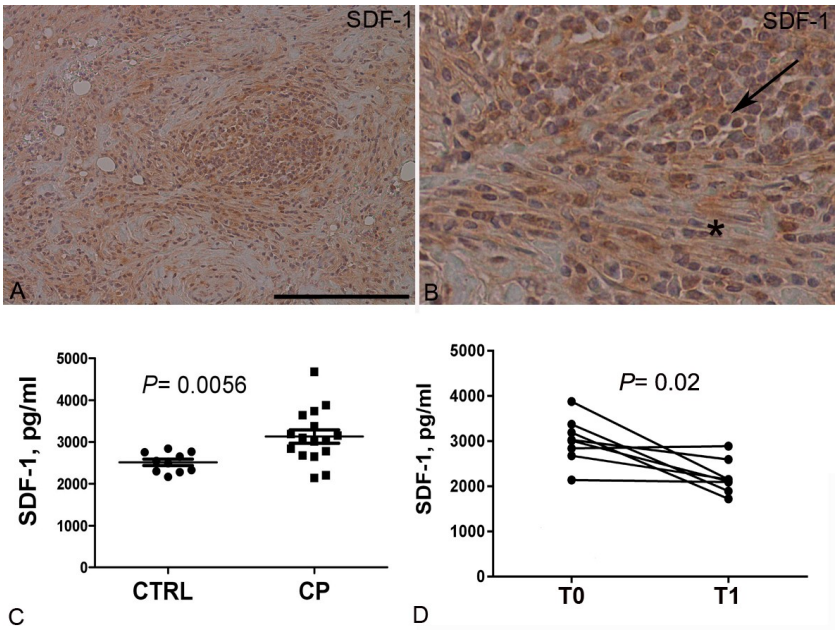

Figure 7. SDF-1. Low-power view (A) and high-power view (B) of an immunohistochemical analysis testing SDF-1 (also known as CXCL12) in a representative case of CP. This marker is positive both in lymphoid cells (arrows) and spindled elements (asterisks). C. SDF-1 ELISA performed in 16 patients with active CP and 10 healthy controls. SDF-1 levels were significantly higher in CP patients than in controls (*P*= 0.0056). D. SDF-1 ELISA performed in 8 patients with active CP (T0) and in the same patients after 1 month of prednisone therapy (T1). SDF-1 serum levels was lower in CP patients at T1 than in patients at T0 (*P*=0.02). Original magnification. A: x20 (bar is 150 µm); B: x63 (bar is 40 µm). Stainings. A, B: immunohistochemical analyses revealed by 3,3'-diaminobenzidine (DAB) and mildly counterstained by Harris hematoxylin

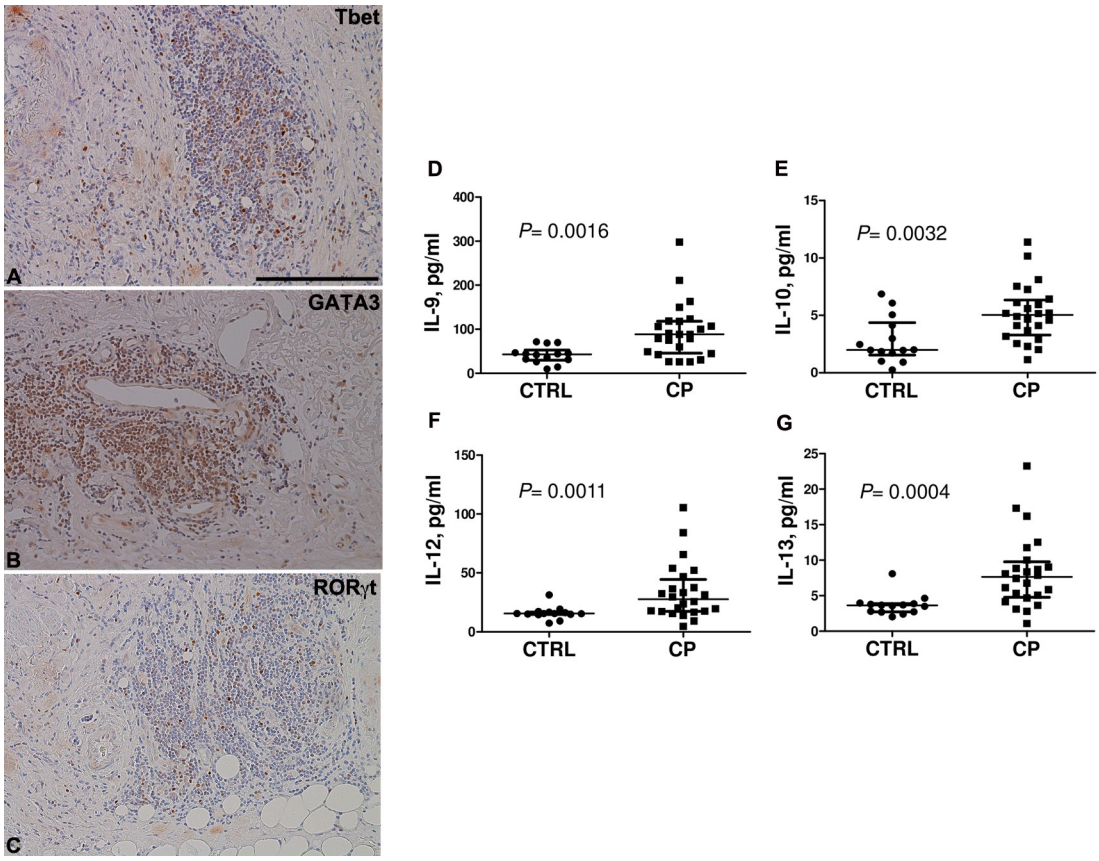

Figure 8. Immunohistochemical detection of T-bet (A), GATA3 (B) and RORγt (C) in inflammatory infiltrates of biopsies obtained from a patient with CP. Serum levels of IL-9 (D), IL-10 (E), IL-12 (F), and IL-13 (G) analysed using a multiplex assay. In each scatter plot, median (bar) and interquartile range are shown. The Mann-Whitney non-parametric test was used for statistical analysis. Considering that multiple cytokines were tested in the same experiment, the cut-off *P* value of 0.05 was corrected using Bonferroni's correction (cut-off P_{corr} 0.0041). Original magnification. A-C: x20 (bar is 150 µm) Stainings. A-C: immunohistochemical analyses revealed by 3,3'-diaminobenzidine (DAB) and mildly counterstained by Harris hematoxylin

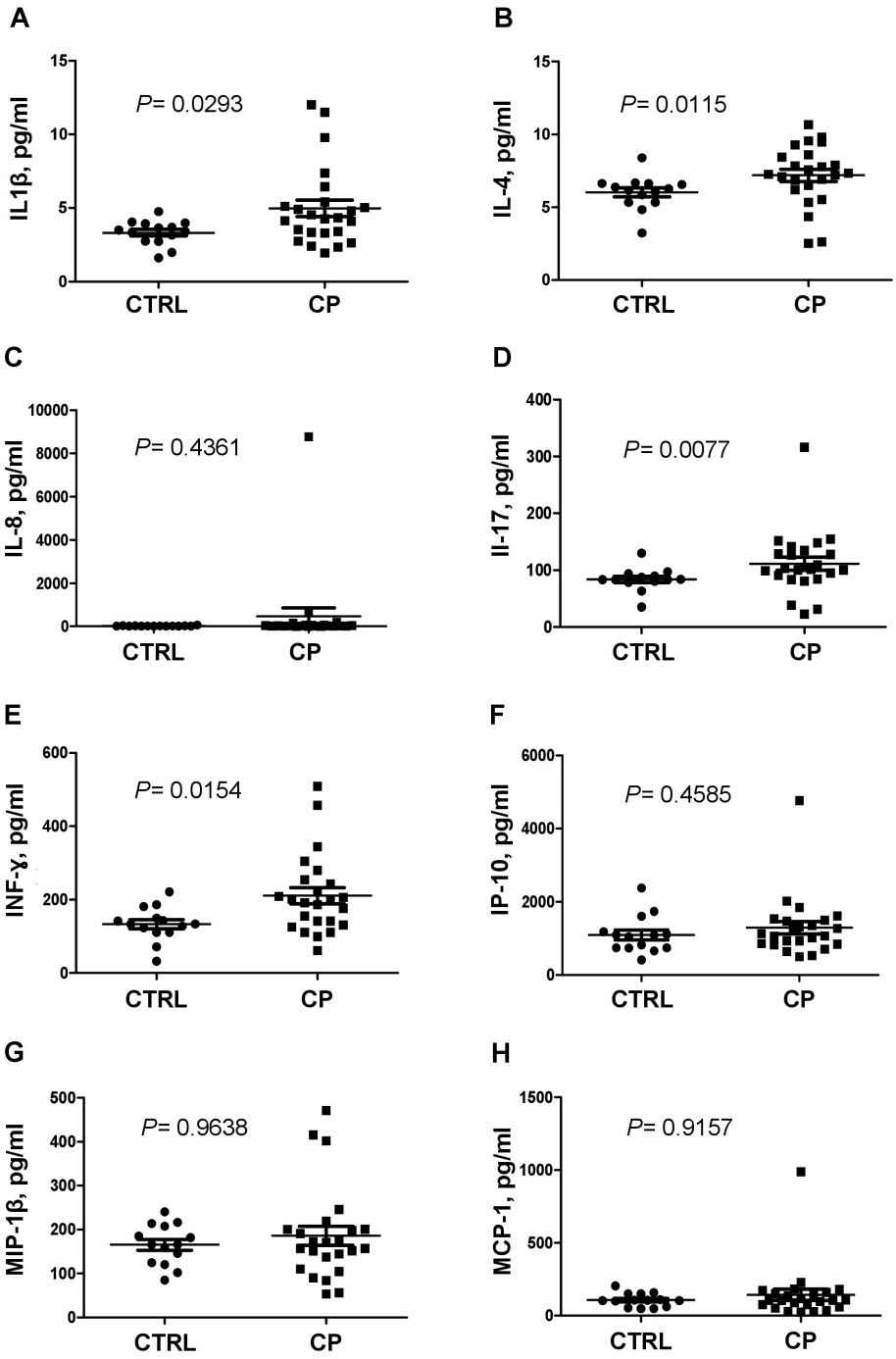

Figure 9. Serum levels of IL1β (A), IL-4 (B), IL-8 (C), IL-17 (D), INF-ɣ (E), IP-10 (F), MIP-1β (G), and MCP-1 (H) analysed using a multiplex assay. In each scatter plot, median and interquartile range are displayed. The Mann-Whitney non-parametric test was used. Considering that multiple cytokines were tested in the same experiment, the cut-off P value of 0.05 was corrected using Bonferroni's correction (cut-off Pcorr 0.0041)